

Drying of thin colloidal films

This article has been downloaded from IOPscience. Please scroll down to see the full text article.

2013 Rep. Prog. Phys. 76 046603

(<http://iopscience.iop.org/0034-4885/76/4/046603>)

View [the table of contents for this issue](#), or go to the [journal homepage](#) for more

Download details:

IP Address: 129.241.220.207

The article was downloaded on 16/08/2013 at 04:26

Please note that [terms and conditions apply](#).

Drying of thin colloidal films

Alexander F Routh

BP Institute and Department of Chemical Engineering and Biotechnology, University of Cambridge,
Pembroke Street, Cambridge CB2 3RA, UK

E-mail: afr10@cam.ac.uk

Received 14 December 2012, in final form 25 January 2013

Published 18 March 2013

Online at stacks.iop.org/RoPP/76/046603

Abstract

When thin films of colloidal fluids are dried, a range of transitions are observed and the final film profile is found to depend on the processes that occur during the drying step. This article describes the drying process, initially concentrating on the various transitions. Particles are seen to initially consolidate at the edge of a drying droplet, the so-called coffee-ring effect. Flow is seen to be from the centre of the drop towards the edge and a front of close-packed particles passes horizontally across the film. Just behind the particle front the now solid film often displays cracks and finally the film is observed to de-wet. These various transitions are explained, with particular reference to the capillary pressure which forms in the solidified region of the film. The reasons for cracking in thin films is explored as well as various methods to minimize its effect. Methods to obtain stratified coatings through a single application are considered for a one-dimensional drying problem and this is then extended to two-dimensional films. Different evaporative models are described, including the physical reason for enhanced evaporation at the edge of droplets. The various scenarios when evaporation is found to be uniform across a drying film are then explained. Finally different experimental techniques for examining the drying step are mentioned and the article ends with suggested areas that warrant further study.

(Some figures may appear in colour only in the online journal)

This article was invited by Athene M Donald

Contents

1. Introduction	2		
1.1. Droplets or films	4	4.4. Criteria for cracking	11
1.2. Coffee rings	4	4.5. Crack spacing	11
1.3. Evaporation rate	4	4.6. Control over cracking	12
2. Non-uniform ‘horizontal’ drying	4	5. Evaporation	13
2.1. Pressure drop in consolidated region	5	5.1. Film pinning	13
2.2. Transitions in drying fronts	6	5.2. Rate of evaporation	13
2.3. Collapse of film under capillary pressure	6	5.3. Large films	13
2.4. Control over colloidal stability during the drying process	7	5.4. Evaporation of droplets	14
2.5. Experimental observation of horizontal drying fronts	8	5.5. Effect of particle volume fraction	15
3. 1D ‘vertical’ drying	8	5.6. Control of humidity	15
3.1. Stratification	9	5.7. Capillary pressure	15
3.2. Experimental studies of 1D drying	10	6. Thin film fluid mechanics	16
4. Cracking	10	6.1. Lubrication theory	16
4.1. Crack types	11	6.2. Effect of volume fraction	17
4.2. Crack dynamics	11	6.3. Effect of surfactant	17
4.3. Crack driving force	11	6.4. Effect of temperature	17
		6.5. Boundary conditions	18
		6.6. Prediction of flow patterns	18

7. Experimental techniques to follow drying in thin films	18	8. Future directions	24
7.1. Microscopy	18	8.1. Evaporative lithography	24
7.2. Following water in a drying film	19	8.2. Control over film topology	25
7.3. Following stress build-up in a film	21	8.3. Varying substrate properties	25
7.4. Measuring film height	22	9. Conclusions	25
7.5. Scattering techniques	23	Acknowledgments	26
7.6. Measuring composition	23	References	26

1. Introduction

Colloidal suspensions are ubiquitous, with common examples being every day products, such as milk and paint. The definition of a colloid involves particles dispersed in a fluid and the particles are small enough to be subject to Brownian motion [1, 2]. This article concerns the process of drying colloidal dispersions and the patterns that are formed.

There has been considerable interest recently in the *coffee-ring effect*, where drying a drop of coffee results in a ring like deposit. This was first reported by Deegan *et al* [3] who provided an explanation based on capillary flow. The largest literature relating to drying of colloidal dispersions comes from the area of polymeric coatings. In the 1960s Sheetz [4] referred to the appearance of horizontal drying fronts passing laterally across drying films of polymeric particles. The physics involved in these horizontal fronts is the same as the coffee ring described by Deegan *et al*: the film is pinned at the edge and drying consolidates the particles at the edge into a solid region. Continued evaporation then pulls fluid and particles from the bulk towards the edge and results in a large horizontal flux. Other examples of patterns during drying of colloidal dispersions include river beds where the periodic wetting and drying leads to developing patterns in the mud [5].

The use of controlled drying is seen within the inkjet printing industry. When an ink drop is placed on a piece of paper a uniform dried droplet is desired. This necessitates minimization of the coffee-ring effect. A complication arises because there are multiple drops within a small area. Consequently, the solvent vapour concentration, above the droplets, is different from the case of a single isolated droplet. An interesting example is described by Wu *et al* [6] where the printing of conductive inks is limited by the formation of coffee-ring like deposits and hence there is the desire to reduce such occurrences.

Issues with drying occur when printing conducting polymers. The lifetime of many conducting polymer displays is proportional to the magnitude of the current which flows. This is determined by the local resistance and consequently the local film thickness. This means that a film with a wildly varying film height will have locally high currents and a shorter lifespan than a flatter film: controlling the final film profile through the drying process is crucial. Van Dam and Kuerten [7] derive equations to predict the final film profile for a sessile drop of polymer containing liquid, subject to evaporation. They also perform white-light interferometry experiments to measure the final profiles in droplets and confirm, at least qualitatively, their numerical predictions.

Another example where control over the drying process is important concerns pesticide drops. When a crop is sprayed with a pesticide, small drops will form on the leaves. There are two possible scenarios and each requires different flow regimes. In one case the active ingredient is required to coat the outside of the leaf and in this case a uniform drying is required, that does not display a coffee-ring effect. In the second scenario the active ingredient is combined with an adjuvant that promotes adsorption of the active ingredient into the leaf. In this case a coffee-ring effect, to concentrate both the active ingredient and the adjuvant in one region of the drop, is advantageous [8, 9].

A further example of drying induced pattern formation concerns polymer containing droplets. A series of papers from Fairhurst discuss the drying of aqueous solutions of poly(ethylene oxide) (PEO) [10–12]. The initial stages of drying for the polymer solution follow exactly as for the colloidal drop case. The coffee-ring formation is observed and the polymer is seen to consolidate at the edge of the droplet. As the solidified region moves towards the centre of the droplet a strange occurrence is observed. The PEO forms a central pillar that increases in height as the drying proceeds. At the end of drying the pillar is above the height of the original droplet. Such drying is only seen to occur for certain evaporation rates and is also a function of the initial polymer concentration and molecular weight. Baldwin *et al* [11] explain the observation with a diffusional argument for the PEO becoming trapped within the drying front. Drying of a different polymer, polystyrene dissolved in anisole, is reported by Kajiya *et al* [13]. They observe a different behaviour, with a transition from a flat dry deposit to a ring like structure as the initial polymer concentration is varied. Head [14] models the deformation of an assumed elastic crust on the surface of a drying film and relates the applied stress to the resulting shape of the droplet. This result shows how the drying behaviour of the droplet will determine the pressure distribution within the water phase and this will, when combined with the mechanical properties of the polymer concerned, determine the dried shape of the drop. Whilst such drying behaviour is interesting scientifically, there are also numerous potential uses for such 3D structures that are created, merely through evaporation. Printed Braille and the use of the towers as anti-slip device for floor coatings are two possible uses.

Once the drying step in a film or droplet is understood and controlled, the assembly of structures becomes possible. Bespoke manufacture of multifunctional materials through a simple, cheap, self-assembly technique is very attractive and the strapline has become to perform 3D printing without the printer! Han and Lin [15] reviewed controlled evaporation

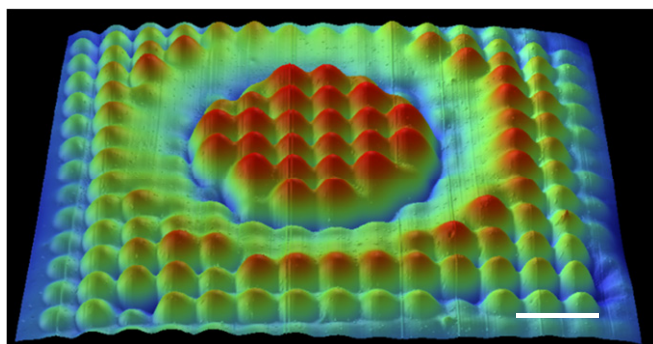


Figure 1. 3D profilometry image from a latex film dried under a mask with holes spaced 1.5 mm apart and the scale bar is 3 mm. The image is reproduced from [20] by permission of the Royal Society of Chemistry.

from droplets and demonstrated how they can control the formation of a number of structures. Harris *et al* [16–18] demonstrated the use of a technique called evaporative lithography. By placing a mask over a drying film, evaporation only proceeds in the uncovered regions. After complete drying the films display humps in the uncovered regions [16]. There are many possible flows in the thin film. These include the evaporative flux towards the uncovered region, surface tension trying to flatten the film and any Marangoni instability arising from the desorption of surfactant from particle surfaces. The fluid mechanics sets the film topology and the different flows within thin films are considered in section 6. In addition different particle types can be used to control composition at different positions within the film. Harris *et al* [18] demonstrate a lateral stratification of a binary colloid mixture upon drying, within the evaporative lithography framework. This is important since it allows control over film composition independently from the film shape. The methods of particle stratification and a model to predict it is described in section 3.1.

Parneix *et al* [19] use an obstacle, placed above a film, to block evaporation in certain regions. The resulting film displayed a dip that corresponds to the original blockage and then ridges as the film height moves away from the central dip. As Parneix *et al* state, this demonstrates a simple technique for templating films on the mm length scale.

The use of evaporative lithography has been developed further recently by Georgiadis, working in the group of Joe Keddie [20–22]. Figure 1 shows a three-dimensional (3D) profilometry image of a film that has been cast underneath a mask of periodic holes. The resulting film has peaks corresponding to the position of the holes, and consequently it is possible to template specific shapes down to a resolution of a few mm. The film in figure 1 is made of an acrylic polymer and during the evaporation stage an infrared lamp was shone through the holes to heat the film. This enabled the latex particles to soften and film-form even though their glass transition temperature is well above room temperature. The technique has been used to template numerous film morphologies including two different length scales by placing one mask with very fine holes above a primary mask with larger

holes. Recent work by Georgiadis *et al* [23] has demonstrated the production of aesthetic coatings for uses such as patterning of candle holders. The important point, with these materials, is that the coatings are made with a single self-assembly step. Utgenannt *et al* [24] have demonstrated the use of evaporative lithography to create a textured surface, combined with particle stratification to arrange gold nanoparticles at specific locations within the film. This creates the possibility of multifunctional textured coatings made through a single processing step.

A slightly different configuration is considered recently by Arshad and Bonnecaze [25]. They consider a film, whose top surface is in contact with a membrane. The thickness of the membrane is spatially variable and hence the diffusion of solvent across the membrane varies with position. This imparts a spatially variable ‘evaporation’ rate that leads to accumulation of particles in regions of largest evaporation. The membrane removes the film air surface and hence the fluid mechanics is greatly simplified. Arshad and Bonnecaze solve momentum and particle conservation equations for the film and the model provides estimates for the spatial resolution of features that can be obtained, with a value as low as 10 nm claimed.

This article is concerned with the drying of colloidal films. These may be small drops, as in inkjet printing, or a large expanse of film deposited on a wall, such as a paint film. The article concentrates on the drying step and the structures that form whilst the film is still wet. The formation of bespoke structures through a single drying step is the ultimate aim of much work around the world, and we aim to collate the relevant literature, from a number of disparate subjects, within this article. We begin by describing the processes that occur when a film is cast and allowed to dry. Numerous transitions are observed and these are explained, mainly with reference to the magnitude of the capillary pressure in the water phase. We spend a lot of time examining the way in which films crack during drying and ways to mitigate such behaviour. To understand the physical processes happening in the controlled assembly, demonstrated by Utgenannt *et al* [24], the arrangement of particles within a drying film needs to be understood and this is examined in a one-dimensional (1D) drying problem. The result demonstrates how to create self-stratifying systems and this is explained. The film topology is controlled by the fluid mechanics during the drying stage and the basic fluid mechanics for thin films is introduced so readers may appreciate the physical processes which contribute to the rich range of flows. Finally some of the experimental techniques that can be used to examine thin films are described.

After consolidation into a solid, a drying film may transform further. In the case of polymeric particles film formation can result in a continuous, clear, mechanically integral film. For non-polymeric particles a processing step will be required to lock the particles within the dry film. This article concerns itself with the drying step and the arrangement of particles into a close-packed material. We do not concentrate on the film formation process and leave that for other reviews [26, 27].

1.1. Droplets or films

Whether drying a $10\ \mu\text{l}$ droplet or a $100\ \text{m}^2$ paint film on an expanse of wall, there are common physical transitions that occur. This article will examine both scenarios and show that there are not too many differences due to the size of the original film. However, one difference that is likely to occur concerns the fluid mechanics. As discussed in section 6 it is usual to employ the lubrication approximation to model surface tension driven flows. This greatly simplifies any numerical flow prediction and whilst this seems eminently reasonable for large expanses of fluid, a small drop, where the aspect ratio is around unity, is unlikely to satisfy the lubrication approximation.

1.2. Coffee rings

The most discussed drying occurrence is of the *classic* coffee ring. The observation is that a drop of coffee, spilt on a kitchen worktop, will dry with the coffee solids in a ring around the original drop shape, and the centre of the drop is seemingly devoid of solids: a flow carries particles to the edge as the drop dries.

The original article that discusses the ring formation is by Deegan *et al* [3] and it has now been cited over 1500 times with over 200 citations in 2012 alone. As will be shown, the coffee-ring, or horizontal drying front, is a common occurrence that is observed when a film has an edge. In large drying colloidal films, the drying front of consolidated particles is seen to traverse across the film and the physics of front formation is the same as in the case of a drying drop.

1.2.1. Why coffee rings form. There are two common explanations for the formation of horizontal drying fronts. Deegan *et al* [3] build on an enhanced evaporation rate at the edge of drying droplets. The droplet remains pinned at the edge and consequently a flow must occur from the bulk of the film to the edge. This carries particles to the edge and causes a close-packed region to form.

An alternative explanation does not rely on an enhanced evaporation rate, and argues that the horizontal drying is observed because of the reduced film height at the edge. Evaporation reduces the film height uniformly across the film and removing solvent from a thin film causes a larger increase in volume fraction than in a thick film. Consequently the volume fraction increases most rapidly at the edge and this results in formation of a close-packed region. The differing views for the formation of consolidated regions at the edge of drying films are considered in section 5.

Irrespective of the reason for a packed region forming at the edge of the film, once formed, evaporation continues from the consolidated region. The evaporation from this solid region causes a flux of fluid from the bulk to the edge and this carries particles with it. The process is sketched in figure 2.

There are many instances when it is favourable to limit the formation of a coffee-ring and different strategies can be employed to achieve this. A recent paper by Yunker *et al* [28] has demonstrated that the use of ellipsoidal particles suppresses the transport of particles to the edge and, as the authors state,

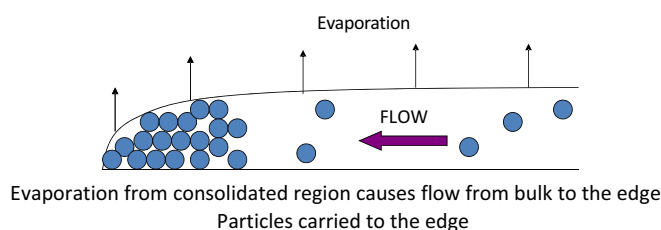


Figure 2. Flows in a drying film.

this will suppress the coffee ring effect. Eral *et al* [29] show that application of an oscillating voltage of 200 V across a drying droplet suppresses the formation of a coffee-ring. The reasons are loss of pinning at the edge of the drop and also creation of flows within the drop that counter the capillary flow towards the edge. Shmuylovich *et al* [30] show that if the film is only lightly pinned then the coffee-ring will form but subsequent de-pinning will lead to multiple ring formation, as the film edge jumps towards the centre, leaving solid deposits behind as it does so.

1.3. Evaporation rate

The entire process of pattern formation in drying films is driven by evaporation. As discussed in section 5 there are many instances where the evaporation rate is a constant per unit area. This is likely to occur in larger expanses of film in non-stagnant air. There are however instances where an enhanced evaporation rate is predicted at curved regions of the film. This is most evident in stagnant air and for highly curved surfaces—such as seen in very small drops. In addition an array of droplets, as commonly occurs in inkjet printing will result in droplets that interact and there will be a minimum evaporation rate in the regions of the droplets that face other drops. This is considered at length in section 5.

2. Non-uniform ‘horizontal’ drying

The drying process for a 10 wt% dispersion of 200 nm diameter polystyrene particles in water is shown in figure 3. The image at zero minutes shows a film that is liquid everywhere. As drying proceeds the film packs into a solid, as shown at the top of the image taken at 40 min. The milky white fluid region shrinks in size but persists to beyond 190 min. The solidified region grows laterally across the film and this region of fluid/solid transition has been termed a horizontal drying front. The solid region constitutes consolidated solid particles that remain under water. The solidified region also displays cracks which propagate into the wet consolidated particles. The final film profile is shown at a time of 250 min and it can be seen how the drying process determines the morphology of the final film.

A number of important questions arise from the drying process in figure 3

Why do horizontal drying fronts form?

How fast do the horizontal fronts propagate?

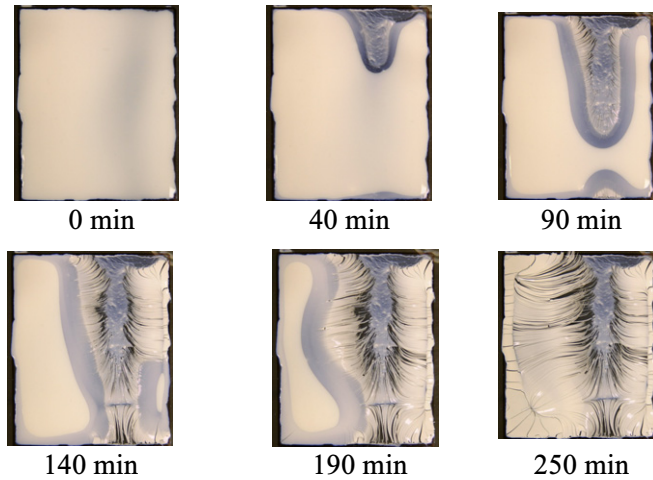


Figure 3. Drying a film of 200 nm polystyrene particles in water. The film is about 30 cm across and has an initial particle loading of 10 wt%.

What causes the film to crack?

What parameters allow control over the final film profile?

The physics of the process and the important parameters to control are investigated in the next sections.

As particles consolidate a number of transitions occur. Figure 4 shows a screen shot from a simple directional drying experiment: polystyrene particles of 115 nm diameter dispersed in water at 10 vol% were spread on a glass slide. Nitrogen gas was blown over the film from the right hand side of the image and the particles consolidated first at the right hand side of the picture. In the image a number of transitions can be seen: the film is still fluid to the left, with particles dispersed in liquid at a volume fraction below close packing. The particles transition into a solid at a solidification front. There are a number of cracks passing through the material and these define a crack front. Finally a drainage front, where the particles become dry and devoid of water is seen at the back of the film.

2.1. Pressure drop in consolidated region

Water continues to evaporate from the consolidated region and hence this water must be replaced, resulting in flow through the solid region. This flow causes the pressure in the water, the capillary pressure, to monotonically decrease along the consolidated region, in a manner sketched in figure 4. To calculate specific values for the water pressure, a constitutive relation, such as Darcy flow, must be assumed. The maximum pressure that can be supported by an array of particles is determined by the surface tension, γ and the particle radius, R . For monodisperse particles the maximum value of the capillary pressure is determined geometrically as $12.9\gamma/R$. A thermodynamic argument [31] leads to the capillary pressure for monodisperse particles, at random close packing, being determined as $5.3\gamma/R$. There are numerous complications in that a particle size distribution will affect the maximum capillary pressure and often the actual particle size is not that well known. The actual magnitude merely appears in scalings

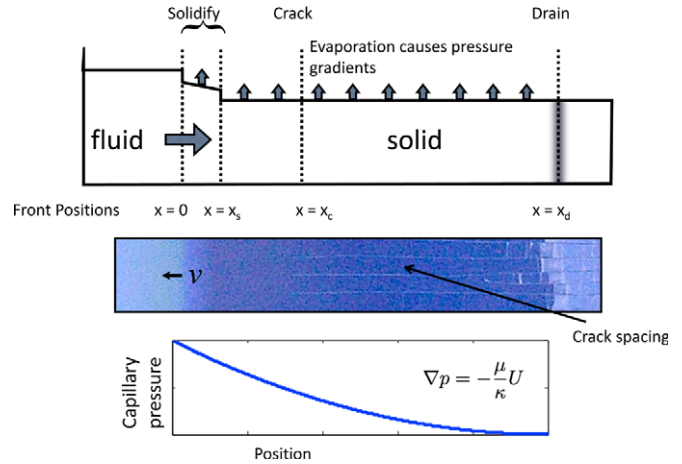


Figure 4. Different fronts form during a horizontal drying experiment. Image drawn by and courtesy of Lucas Goehring.

and so for simplicity we take the maximum capillary pressure as $10\gamma/R$.

The pressure drop along the consolidated region is determined by the magnitude of the evaporation rate and the permeability of the solid region. This magnitude must be compared with the maximum capillary pressure. If the maximum value is never reached then the water will continue to flow to the edge of the film and the particles will remain saturated with water. Conversely, if the maximum capillary pressure is reached then the water pressure will saturate at this maximum value, and a stagnant region will form. Evaporation will then remove water, which will be observed to recede from the edge of the film. The ratio of the maximum allowable capillary pressure to the value achievable, is called the dimensionless capillary pressure [32, 33] and is given by

$$P_{\text{cap}} = \frac{20}{75} \left(\frac{3\gamma\eta_0}{\dot{E}} \right)^{1/2} \frac{R(1-\phi_m)^2}{\mu\phi_m^2 H}, \quad (1)$$

where η_0 is the dispersion low shear viscosity, \dot{E} is the evaporation rate, ϕ_m is the volume fraction of particles at close packing, μ is the solvent viscosity and H is the initial film thickness.

The importance of this dimensionless group was examined experimentally by Salamanca *et al* [33]. Using two-dimensional (2D) magnetic resonance imaging (MRI) measurements they tracked the position of water in a drying film and determined the time at which water receded from the edge of the film. For high values of P_{cap} the maximum capillary pressure is never reached and water continually wicks to the edge of the film. For lower values of P_{cap} the water saturates at the maximum capillary pressure, and consequently water recedes from the film edge. This simple fluid mechanical view allows prediction of the *open time* of a film, or the time during which a film may be touched-up or reapplied. Figure 5 shows two contrasting MRI images for low and high values of P_{cap} . For $P_{\text{cap}} \gg 1$ it can be seen that the water remains pinned at the edge of the film throughout the drying and the open time is long. For $P_{\text{cap}} \sim 1$ the water is seen to recede from the edge. The results from all the experiments of Salamanca *et al*

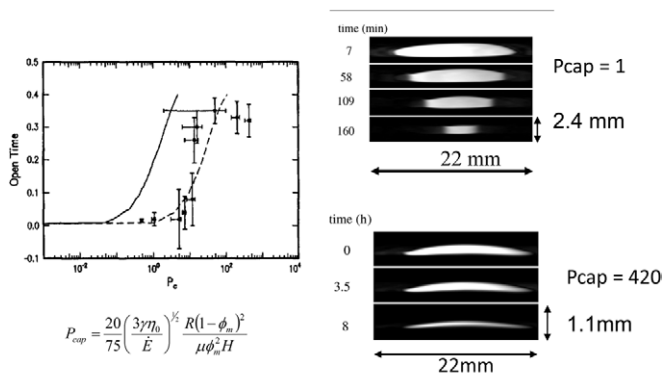


Figure 5. Measured and predicted open time for a film drying horizontally. Included are 2D MRI images of drying film where the white colour shows the presence of water. Reprinted with permission from [33]. Copyright (2001) American Chemical Society.

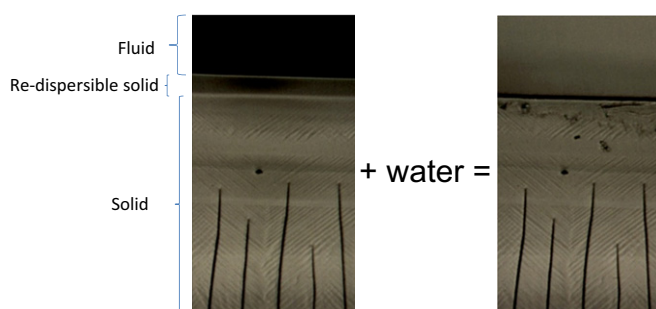


Figure 6. Microscope image of a solidification front. Upon addition of water a region becomes redispersed, indicating reversibility in the packing. Images courtesy of Lucas Goehring.

are shown in figure 5. In this figure the open time corresponds to the time at which water recedes from the edge of the film, normalized by the total evaporation time and the transition in open time around a P_{cap} value of 5 is seen.

2.2. Transitions in drying fronts

Figure 4 shows a number of fronts propagating across the drying film. We now consider each of these transitions in turn.

2.2.1. Solidification front. The first transition involves particles changing from a liquid to solid state. This can be seen as a gradual change in shade in figure 4. Goehring *et al* [34] synthesized monodisperse polystyrene latex particles to examine the solidification front. Figure 6 shows a microscope image of the packing front. It is interesting to note that upon addition of water some of the consolidation front redisperses. This implies that the particles are held in a secondary minima and have not irreversibly aggregated. Using suitably sized particles, the spacing between particles can be made to diffract visible light and hence result in a colour change, this is shown in figure 7. The redispersible part of the transition shows as green with the irreversibly aggregated particles displaying as blue.

Goehring *et al* [34] followed the width of the reversible region and demonstrated that the width multiplied by the front velocity was a constant. Because the front velocity

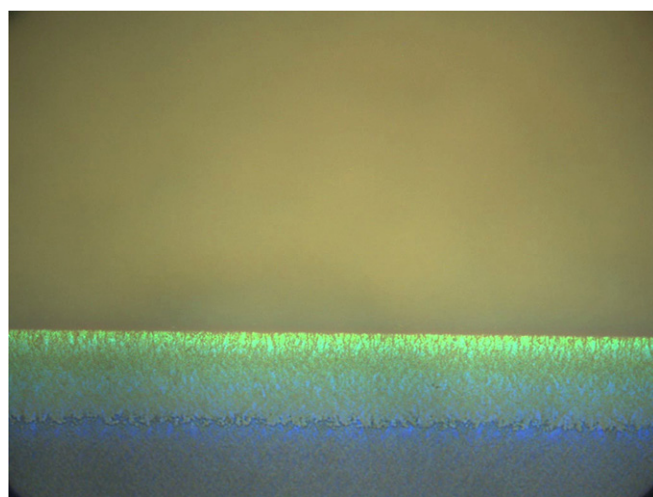


Figure 7. As consolidation front passes through film a colour change is seen indicating a change in particle packing. Image reprinted with permission from [34]. Copyright (2010) American Chemical Society.

is proportional to the fluid pressure gradient, the result of Goehring *et al* indicates that the transition to irreversibility followed a line of constant pressure. This suggests that the particles are first brought into a close-packed array where an electrostatic repulsion maintains a certain separation. As the capillary pressure builds up the particles eventually move into contact and irreversibly aggregate. Therefore the transition from reversible to irreversible contact allows simple measurement of the maximum in the inter-particle potential between particles. Goehring *et al* [34] demonstrated this with the addition of salt to lower the maximum potential between particles and consequently lower the pressure needed to cause irreversible contact.

2.2.2. Crack front. Some way behind the solidification front follows a crack front. This is shown in figure 4 and it can be seen that the cracks display a well-defined spacing. A further image in figure 8 shows a film comprising 400 nm polystyrene latex particles and an array of propagating cracks can be seen. The issue of cracking in drying films is considered at length in section 4.

2.2.3. Dewetting front. The capillary pressure decreases monotonically along the compacted region of the film. Once the capillary pressure reaches its largest attainable value the water pressure saturates and the water can no longer flow to the edge of the film. This allows the film to become dry and a drainage front is seen. This is visible to the right of the film in figure 4.

2.3. Collapse of film under capillary pressure

In the case of soft, film forming, latex particles a further transition can be observed during drying. An optical clarity front can pass laterally across the film, some way behind the particle compaction front [35]. In this case the soft particles deform in response to the capillary pressure and so no cracks

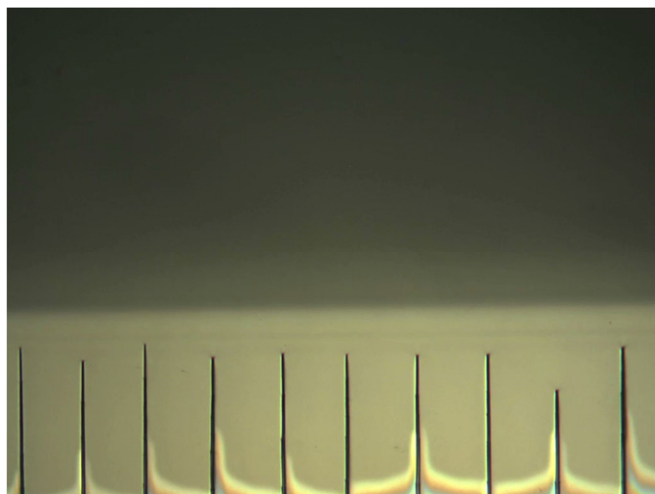


Figure 8. Cracks propagating through a drying film of 400 nm polystyrene latex particles. Notice the regular crack spacing and how the cracks lag a set distance from the solidification front.

are observed in the film. Once the voids between particles became much smaller than the wavelength of light, the film becomes clear. Routh *et al* [35] used a model for particle deformation under the spatially varying capillary pressure to predict the onset of the optical clarity front. An alternative approach, that has not yet received attention, is to use the capillary pressure to collapse a colloidal gel, which would initially form at the edge of the film. A possible system to achieve such behaviour is shown by Hodges *et al*, who dry droplets containing laponite clay, and the system gels as the particles consolidate [36]. This way the final film shape will be determined by the strength of the particle network in comparison to the available capillary pressure.

2.4. Control over colloidal stability during the drying process

An attractive way to control the arrangement of particles within a drying film is through colloidal stability. If the particles can be transitioned to an unstable state, at some point in the drying process, they will aggregate and fall out of solution. The advantage of such a scheme would be that any subsequent flows, in the drying film, will likely have no effect on the final film morphology. The counter side is that any coating is desired to be stable during storage and so it is necessary to store a dispersion far away from any stability boundary.

An elegant example of colloidal destabilization during film drying is given by Haw *et al* [37]. The authors used sterically stabilized monodisperse poly(methyl methacrylate) particles in decahydronaphthalene with polystyrene added as a free polymer. The polystyrene introduced a depletion attraction between the particles and consequently, upon drying, the dispersions traversed the colloidal phase diagram, passing from a region that the phase diagram predicts to be a colloidal fluid, into a phase separated region and finally into a gelled region. As the authors point out the phase diagram is for bulk samples at long time and the drying process is necessarily a non-equilibrium process so that drying films may not display

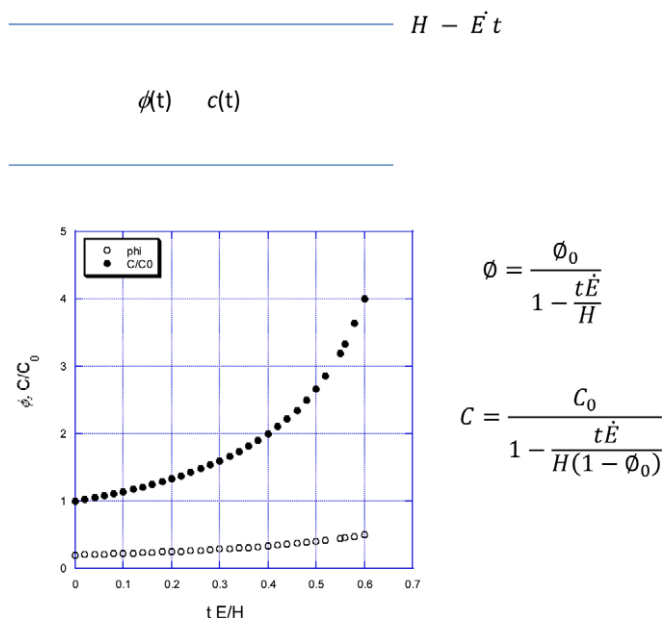


Figure 9. A film of original thickness H evaporating at a rate \dot{E} will experience an increase in average particle volume fraction, ϕ and salt concentration C .

the equilibrium phases. Haw *et al* [37] observed a remarkable range of drying patterns, dependent on the phase diagram, the rate of drying and the rheology of different colloidal phases.

The *classic* way to destabilise an aqueous colloidal dispersion is through the addition of electrolyte. This will screen the electrostatic repulsion between particles and above a critical concentration the particles will rapidly aggregate [2]. The easiest thought experiment involves a salt concentration in the original dispersion that is below the critical coagulation concentration. Drying will increase the *average* salt concentration and hence transition the film into the unstable state. There are a few problems with this simple experiment: the salt and particles will be inhomogeneously distributed throughout the film, resulting in only certain regions of the film that are colloidally unstable. More importantly though, control over such a drying process is difficult. Figure 9 shows a sketch of a film of initial height H evaporating at a rate \dot{E} . If the particles and electrolyte are assumed to be evenly distributed across the film, simple mass balances give expressions for the particle volume fraction and salt concentration in the film, as shown. Figure 9 also graphically shows the evolution of salt concentration and volume fraction for an initial particle volume fraction of 0.2. The salt concentration reaches four times its initial value when the particle volume fraction has reached 60%. This implies that such a system would need an initial salt concentration of at least 25% of the critical coagulation concentration. More realistically, to achieve destabilization early in the drying process, say before the average volume fraction reaches 33% the initial salt concentration must be 50% of the critical value. Such a formulation would be impractical for a commercial dispersion that requires storage for an extended period, although for a lab experiment it is feasible to envisage such a set-up. Such a scenario will be most useful when drying very dilute dispersions, since this

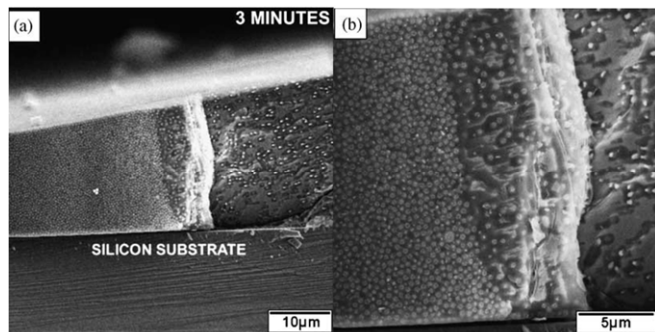


Figure 10. Cryo-SEM image of a horizontal drying front in a film comprising 500 nm diameter polystyrene particles in water. Reproduced from [38] with permission from Elsevier.

provides the longest time to achieve a destabilization. Despite the simplicity of such an experiment, other than the references in section 4.6.3 relating to crack morphologies, no reports were found that use electrolyte to controllably cause colloidal aggregation during the drying process.

2.5. Experimental observation of horizontal drying fronts

Direct observation of horizontal drying fronts can be easily carried out by eye, with changes in the film appearance and texture seen to sweep across drying films. To examine such transitions on the particulate length scale is more difficult. To visualize 100 nm length scales requires the use of electron microscopes and this negates the possibility of *in situ* examination. A cryo-scanning electron microscopy (SEM) image of a horizontal drying front is given by Ma *et al* [38] and this is reproduced in figure 10. The technique is attractive because it provides a direct image of the particle arrangement.

The major consequence of horizontal drying fronts is the pressure gradient that develops across the film. This manifests itself through film cracking, as discussed in section 4. The stress in the film can be measured in a variety of ways as discussed at length in section 7.3. One possible technique is beam bending [39–42], and typical results show a build-up of stress followed by a dramatic decline. The build-up has been ascribed to capillary pressures developing and the rapid decline to crack formation. It is then common to take the maximum measured stress and assume that this is the yield stress of the drying film [41].

3. 1D ‘vertical’ drying

As seen in section 2, a drying film will display horizontal drying fronts. However, for a large expanse of film, well away from an edge, the lateral flow will not be relevant and the film will be seen to dry one-dimensionally. There are many observations of such drying and vertical inhomogeneities in drying films are often observed during domestic DIY. An early literature report of such an occurrence is due to Sheetz [4] who reported the formation of a skin layer at the top of a drying paint film. This layer hindered further water evaporation and slowed the entire film formation process. The conceptually simple problem of an infinite expanse of fluid evaporating from the top surface has

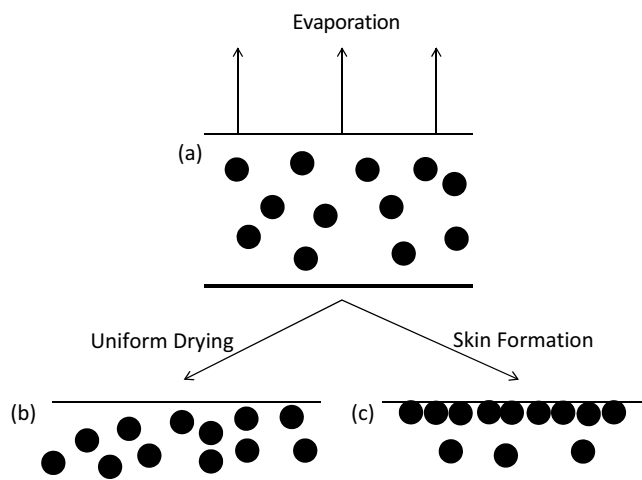


Figure 11. 1D ‘vertical’ drying of a film. An initially uniform particle profile (a) upon drying can either stay well distributed (b) or form a skin at the top layer (c).

been examined by a number of authors. Figure 11 sketches the physical picture with the initial condition of a uniform film evaporating from the top surface shown in figure 11(a). Vanderhoff [43] measured the evaporation rate from a latex dispersion and showed that the rate of mass loss is the same as for a pure water film, until the particle volume fraction reached close packing. Vanderhoff assumes that the particles are uniformly distributed throughout the film, as sketched in figure 11(b). Croll [44, 45] showed, for a different system of aqueous acrylic latex, that the initial rate of mass loss was 85% of the loss from pure water. Croll introduced a conceptual view of a dry top layer of the film, through which water vapour must diffuse. This dry layer increases in size as the drying proceeds and consequently leads to a decrease in evaporation rate with time. The scenario is sketched in figure 11(c).

To predict the evolution of particle volume fraction during the drying process Reyes and Duda [46] performed a Monte Carlo simulation. The results demonstrated that under a slow enough evaporation rate the particles are able to crystallize, whilst for a faster evaporation a random packing is predicted.

Routh and Zimmerman [47] modelled the drying step by writing a diffusion equation for the particles. The concept is that strong diffusion will lead to a uniform film profile, whilst weak diffusion will lead to skinning. The particles of radius R with diffusion coefficient D_0 are contained in a film of initial thickness H and the top surface reduces at a rate \dot{E} . This imposes an evaporative time H/\dot{E} on the system. There is also a diffusive time, H^2/D_0 . If the time for diffusion is much larger than the time for evaporation ($H\dot{E}/D_0 \gg 1$) then the system displays skinning. The opposite case, where the time for diffusion is short ($H\dot{E}/D_0 \ll 1$), leads to a uniform volume fraction profile. The dimensionless group $H\dot{E}/D_0$ is called a Peclet number, denoted as Pe , and after substituting for the Stokes–Einstein diffusion coefficient the Peclet number is given by $Pe = (6\pi\mu RH\dot{E}/kT)$. One prediction from the work of Routh and Zimmerman is that for large Peclet numbers the gradient in volume fraction profile through the

film ($d\phi/dz$) scales as $Pe^{0.5}$. This was tested experimentally by Ekanayake *et al* [48] using magnetic resonance profiling. They found that the gradient scaled as $Pe^{0.8}$. The discrepancy could be down to experimental scatter or, as the authors argue, that the skin formation lowers the evaporation rate and this is not in the model of Routh and Zimmerman. Narita *et al* [49] examined non-uniformity in drying concentrated dispersions. In qualitative agreement with the Peclet number argument of Routh and Zimmerman they found that thick films and high evaporation rates lead to non-uniform films. They however report a discrepancy in that films with high Peclet numbers were found to dry uniformly and the reason was ascribed to the use of the Stokes–Einstein diffusion coefficient in the Peclet number definition. Narita *et al* [49] propose that for concentrated dispersions the transport of water by flow through a permeable bed is the relevant diffusive timescale and this modified Peclet number gave a far better fit to their data. An alternative approach is to modify the time available for evaporation by the ratio of the starting volume fraction to the volume fraction at close packing and this will drastically reduce the Peclet number for concentrated dispersions. König *et al* [50] investigated the effect of added salt and demonstrated that higher salt concentrations lead to skin formation. A possible explanation is provided by Sarkar and Tirumkudulu [51] who show how the charge on colloidal particles enhances the particle diffusivity and hence alters the volume fraction profile during drying. Another way to alter the diffusion coefficient of colloidal particles is with free polymer and Buss *et al* [52] demonstrate how addition of PVA to a silica water solution lowers the diffusion coefficient and effectively increases the Peclet number, enhancing non-uniform drying.

An interesting application of skin formation is demonstrated by Shimmin *et al* [53]. By controlling the evaporation rate, a skin layer of particles is generated. In addition, adding fresh solvent to the bottom of the film extended the drying time and the skin layer was made to crystallize. Shimmin *et al* suggest that such a drying technique is a way to manufacture colloidal crystals. Cardinal *et al* [54] extended the model of Routh and Zimmerman to include sedimentation. This enabled creation of 2D drying maps to show regimes where diffusion or sedimentation dominate the observed microstructure. Experimentally Cardinal *et al* used cryo-SEM to examine a number of film cross-sections and hence experimentally obtained points for their drying maps, that are in agreement with their theoretical predictions. The experimental details are discussed in section 7.1.2.

3.1. Stratification

Control over volume fraction profiles during the drying process opens the possibility of self-stratification in drying films. The simplest case is sketched in figure 12, where a film containing two types of particle is dried. The resulting film may then display one particle type on top of the other. There are many possible driving forces to achieve the stratification. Trueman *et al* [55, 56] proposed a model balancing particulate diffusion with the enforced evaporation rate. Similarly to the single component Peclet number argument of Routh and Zimmerman,

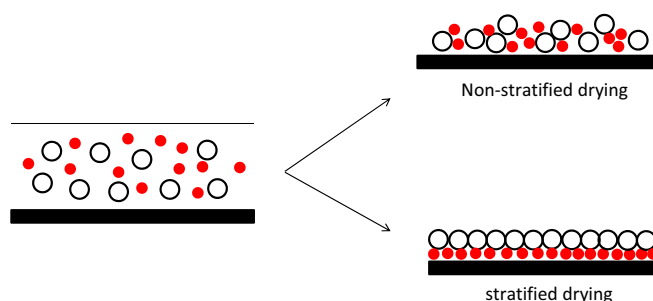


Figure 12. A film containing two types of particle can either dry uniformly or display self-stratification.

Trueman *et al* define two Peclet numbers, one for each of the components. When one Peclet number was above unity, and the other below, then stratification was predicted. Trueman *et al* also observed the predicted stratification using atomic force microscopy (AFM) to sample the top surface of a film and MRI to examine through the film thickness [56]. Atmuri *et al* [57] extended the work of Trueman *et al* to include an interaction between the particles. They demonstrated that when a particular particle type has an affinity for the top surface, a surface enrichment is observed. There are many ways to affect the diffusion coefficient of colloidal particles and an elegant method is charge. Nikiforow *et al* [58] demonstrate, using confocal microscopy, how particles of the same size but different charge will display a stratification upon drying. The explanation proposed by Nikiforow *et al* is similar to the argument of Trueman *et al* [55] but Nikiforow *et al* introduce a collective diffusion coefficient to account for the effect of the varying surface charge. A different stratification mechanism is proposed by Luo *et al* [59]. They dried 550 nm diameter latex particles blended with ceramic nanoparticles. A range of ceramic particles were tested with silica, alumina and antimony doped tin oxide employed. The small particles had diameters ranging from 7 to 45 nm and an accumulation of the ceramic nanoparticles at the top surface of the film was observed. The mechanism, that the authors propose, is that the latex particles form a top layer on the drying film. This is because of the large Peclet number for the latex particles. Continued drying, forces water through the interstices between the large latex particles and this carries the small ceramic particles up to the film surface. The stratification is therefore dependent on the size differential between the two particle types being larger than about 6.5, to allow the passage of the small particles, and also a sufficiently large Peclet number for the large particles, so as to create the top surface of consolidated particles.

3.2. Experimental studies of 1D drying

The 1D drying of films has been examined using a variety of experimental techniques. Probing the top layer of the film has the advantage of simplicity, although there is always the question as to how representative the top surface is, with relation to the bulk. In addition care must be taken to ensure sufficient lateral sampling to account for any inhomogeneities in the film surface. Techniques such as tapping mode AFM allow surface profiles to be measured over lateral distances

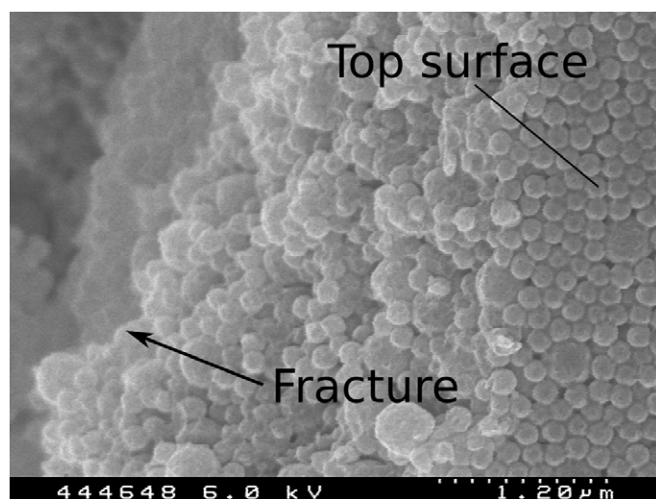


Figure 13. Cryo-SEM image from an almost fully dried bi-modal film. Notice the extra accumulation of small particles on the film surface and how the top surface is not representative of the volume fraction profile across the film. Image reprinted with permission from [57]. Copyright (2012) American Chemical Society.

of around $5\text{ }\mu\text{m}$ [60,61]. The technique allows for easy identification of different sized components at the surface [56]. In addition phase images can show different compositions on a film surface [60]. Surface composition can also be inferred using many surface reflectance techniques such as TOF-SIMS [61] or FTIR [62]. The crystallinity of particle packings are often of interest and this has been followed by Dingenouts and Ballauff [63] using small angle x-ray scattering (SAXS).

Measurements of the particle volume fraction profiles through the film are harder to achieve. Cryo-SEM requires freezing the film at a specific point during the drying process, fracturing and imaging the cross-section. Atmuri *et al* [57] display a cryo-SEM image of a film comprising two particle types. The image is reproduced in figure 13 and Atmuri *et al* demonstrate that the top surface can be anomalous with regards the accumulation of one particle type. Hence the need for techniques that provide information throughout the film depth. A beautiful series of images showing a consolidation front propagating through a film are shown by Ma *et al* [38], and these are reproduced in figure 14.

Gradient-at-right-angles-to-field (GarField) nuclear magnetic resonance (NMR) imaging provides the opportunity to image the water content of films *in-situ* as they dry. The technique has been used extensively to examine the 1D drying of films, looking at skin formation [64, 65] and even cross-linking reactions within films [66]. Details of GarField NMR are described in section 7.2.2.

4. Cracking

As seen in figure 4, an array of cracks can pass laterally across a drying film. The cracks display a characteristic spacing and propagate in a stick-slip fashion. There is a rich debate about the stress and material response leading to the observed cracks and these are examined in this section. The interest in controlling such behaviour arises because particle self-assembly is limited by the size of structures that can be formed

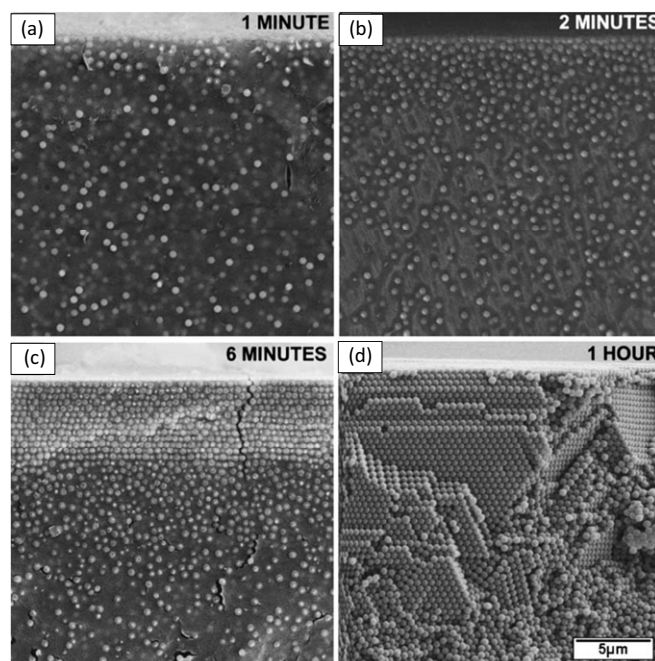


Figure 14. Cryo-SEM images showing a consolidation front passing vertically through a film that comprises 500 nm diameter polystyrene particles in water. Images are reproduced from [38] with permission from Elsevier.

during the drying step. As discussed by Juillerat *et al* [67] and Zhou *et al* [68], the formation of colloidal crystals for use in photonic band gap materials is limited by the ability to dry such materials and the formation of cracks. A further interest arises in the crack patterns that form in oil paintings, which are called craquelure. These cracks can be used to identify the age and origin of oil paintings [69, 70] and the use of craquelure can also help identify art forgeries [71].

As will be discussed below, the question of cracking in thin films has been an active area for a number of years [72]. The recent interest has followed the work of Chiu and Cima [73, 74], who dried aqueous alumina dispersions. They demonstrated that films needed to be above a certain thickness to display cracks. This is called the critical cracking thickness. A further result was the need for a substrate constraint to induce cracking: when films were dried on a pool of mercury no cracking was observed. Recent work by Smith and Sharp [75] used a range of substrates with increasing modulus and Smith and Sharp found that weaker substrates led to a larger crack spacing.

Whilst most work has examined simple spherical latex particles, other particles will also crack upon drying. Tarafdar demonstrate a cracking study using laponite clay [76] and Goehring *et al* used bentonite clay [34].

4.1. Crack types

The images in figures 4 and 8 show straight cracks propagating directly across a film. There is an extensive literature on different crack morphologies with reports of spirals [77, 78], oscillatory [79], circular [80] and arched cracks [81]. Some representative images of different crack morphologies from

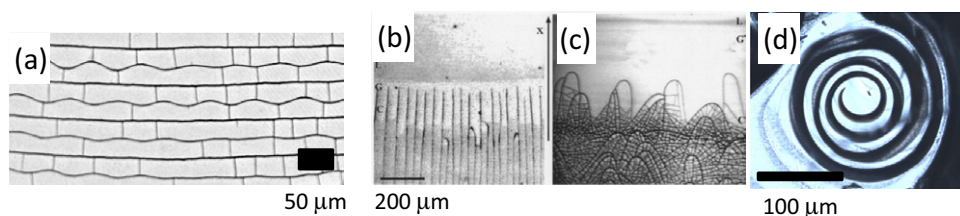


Figure 15. Different crack morphologies. (a) Wavy cracks observed in a film comprising polystyrene latex. The film thickens and hence the desired crack spacing varies with position. (b) a straight array of cracks and (c) arched cracks. The difference between samples (b) and (c) is the particle size with sample (b) having a particle diameter of 100 nm and sample (c) a diameter of 20 nm. (d) Spiral cracks are observed at late times in thick films. Notice the different scale bars. (a) reproduced from [79] with permission from the Royal Society of Chemistry. (b) and (c) from [81], copyright (2003) by the American Physical Society, and (d) from [78] with permission from the Royal Society of Chemistry.

dried particulate films are shown in figure 15. The directional growth due to the horizontal drying leads to a direct analogy with cracking of glass that is rapidly quenched, leading to a thermal strain. In the case of quenched glass a similar range of crack morphologies are observed [82–89].

When a film dries in a more uniform stress field, such that directional drying is not relevant, a different crack pattern is observed and this is often referred to as mud cracks [5, 90–92] or isotropic drying [93]. There have been numerous attempts to classify the structures formed [94–96]. In an interesting development Tirumkudulu and Russel [40, 97] observed a film displaying horizontal drying fronts. The film however did not display any cracks until the entire film had consolidated and then a brittle fracture like morphology was seen. Similar patterns were observed by Holmes *et al* [98], although in their case the cracks did follow the drying front. It seems likely that the stress field, generated by the drying fronts, determine the crack morphology. Hence the drying process determines the resultant film.

4.2. Crack dynamics

The dynamics of cracking shows a staircase progression with the cracks seemingly not moving, followed by a rapid jump and then a further period of rest. This was observed and explained by Dufresne *et al* [99, 100] using a stick-slip type mechanism. In their model a critical stress is needed to initiate crack growth and the crack propagates into the film and regions of lower stress. At some second critical stress the motion stops and the crack then waits for the stress to build up, and the process repeats.

4.3. Crack driving force

The most fundamental question arises from what stress causes the film to crack. This was answered by Dufresne *et al* [99] who demonstrated that the film remained wet at the point of fracture. The result is unambiguous proof that the capillary pressure is responsible for cracking the film. The confusion arises because the capillary pressure is negative implying that the film is under compression yet seemingly fails by a brittle fracture. The answer lies in the substrate constraint highlighted by Chiu *et al* [73] and shown schematically by Lei *et al* [101, 102]: as the capillary pressure builds up the film wants to contract. It can do this normal to the substrate but it is constrained

horizontally, by shear stresses from the substrate. The only way the in plane stress can be relaxed is through generation of cracks.

4.4. Criteria for cracking

The failure of elastic materials is usually explained by an energy balance, where the elastic energy gained, by relaxing the material, balances the energetic cost of creating new area in the crack face [97]. There is extensive literature available for the fracture of thin elastic layers subject to a stress [103, 104]. For drying films the process is more complex because the material properties develop as the particles consolidate, and hence a single elastic modulus may not be appropriate. In addition, even the assumption of elasticity has been questioned [105]. Irrespective of the material response the concept of an energy balance is a common theme to most available models for the onset of cracking [106–108].

4.5. Crack spacing

The experimental observation of an ordered crack array leads to the question of what sets the crack spacing, and this has been debated extensively. One strand of literature assumes a thin elastic film bonded to a substrate, subject to a known axial stress [109–117]. For drying coatings the issue is that the stress at fracture is unknown. One limit is to solve for the stress that will produce a single crack in an infinite medium. Alternatively the crack front can drop back further from the solidification front and this results in a higher stress, and consequently a higher density of cracks. There is a locus of energetically equivalent results that couple acceptable stresses to crack spacings. Tirumkudulu and Russel [97] refer to this as the over pressure, with a higher pressure leading to a higher density of cracks.

The same problem arises in a glass slide being thermally quenched. In this case conduction of heat away from the crack face can determine the spacing [87]. This is known as a selection rule to determine the observed regular spacing. For drying films the same issue arises, in that a selection rule is required to specify a particular solution. One possible selection rule was proposed by Lee and Routh [118] who suggested that flow of solvent away from a crack as it opens, sets a hydrodynamic distance. This distance then sets the crack spacing.

An alternative explanation is put forward by Jagla [119]. He argues that cracks will form at positions of weakness in the film and then propagate. Hence the number of cracks will be set by the number of defects and the cracks will repel each other to give a uniform spacing. The crack front will then position itself to have sufficient stress to support the crack spacing imposed on it. The work of Goehring *et al* [79] however demonstrates that some cracks stop their progression, as a film thickens. This results in an increasing crack spacing despite a higher crack density being initially imposed on the film.

Experimental studies for drying dispersions were shown by Allain and Limat [120]: placing a dispersion between two glass plates ensured evaporation from only one end and consequently a progression of cracks from the exposed end into the bulk. Allain and Limat extracted a crack spacing and showed that this scaled with the film thickness. The drawback of the experiment is that the film is constrained on both the bottom and top surface, inevitably changing the boundary condition from the single substrate case. However, the simplicity of the experiment has led to it being repeated by a number of groups [99, 121, 122].

4.6. Control over cracking

Industrially, coatings are required to dry without displaying any cracks. As discussed above hard particles will ubiquitously fracture due to the capillary pressure induced during drying. There are numerous processing parameters however, that can be used to limit the observed cracks.

4.6.1. Temperature. When drying polymeric particles it is possible to raise the temperature above the glass transition temperature of the polymer. The particles become soft and any applied stresses are dissipated by deformation of the particles, rather than crack formation. As a consequence, when drying latex films at different temperatures, it is observed that the crack spacing increases with increasing temperature and no cracks are observed above a critical temperature, called the crack point minimum film formation temperature [123].

Whilst tempting to always dry polymeric coatings above the glass transition temperature, the resulting film will be tacky and subject to flow. Therefore it is common to add coalescing aids to paint formulations to lower the glass transition temperature of the polymer during drying. These coalescing aids then evaporate, over a few days, to leave a hard crack free coating [26]. Legislation is restricting the use of coalescing aids because they are a volatile organic compound (VOC) and contribute to air pollution and global warming. Hence other methods to avoid cracking in drying films are desired.

4.6.2. Film thickness. The concept of critical film thickness is well known: a film must have a sufficient thickness to display cracks. The reason is that as films become thinner the elastic energy recovered by cracking is not sufficient to propagate a single crack. This was quantified by Singh and Tirumkudulu [124] who derived an expression for the critical thickness and

experimentally confirmed their predictions. Hence it may be feasible for a particular application to use a very thin film and avoid the problem of cracking.

4.6.3. Inducing particle aggregation during drying. The mechanical response of an array of particles is closely related to the particle arrangement. Consequently controlling dispersion stability offers a way to control the mechanical response of the dried solid. This was exploited by Singh *et al* [125], using an aqueous alumina dispersion and altering pH to affect the close-packed volume fraction of dispersions. They observed an effect on the critical cracking thickness of the film. Pauchard *et al* [126] dried films with different salinities. The varying salt concentrations leads to differing levels of colloidal stability and, as expected, different crack patterns were observed depending on the salt concentration. The results however were complicated by effects of salt on the surface tension driven flow in the drying drop. This manipulation of colloidal stability was mentioned earlier in section 2.4.

4.6.4. Polymers. It is reported by Kanai and Sawada [127] that crack free films can be obtained by inclusion of a hydrogel network within the drying film. The reason for this seems to be twofold: the cracks in films occur in response to the capillary pressure. If the particles in the film are held a distance apart then the capillary pressure will not be so large. Consequently the driving force for cracking is reduced. In addition the polymer network provides a soft medium that can deform in response to any stress and hence relieve the stress without crack formation. Kanai and Sawada [127] demonstrate that crystalline regions can be formed, with the material then surviving drying. The spacing between particles is controllable with the molecular weight and amount of added polymer.

4.6.5. Particle blends. Because soft particles will readily deform due to any capillary pressure, and not display cracks, the use of particle blends is attractive. In this scenario soft particles will deform and relieve any applied stress, whilst hard particles will provide mechanical stress to the resulting film. This was examined experimentally by Tzitzinou *et al* [128] who showed that a coherent crack free film is formed when a continuous network of soft particles is created. Singh *et al* [129] modelled the interaction between particles of different moduli to predict the stress strain behaviour of a film containing particle mixtures. They also measured the stress in the film during the drying process using a cantilever method, as discussed in section 7.3.1. Similarly to Winnik and Feng [130] they observed that the stress evolution became sharper as the number of hard particles in the film increased.

As discussed in section 3.1, a problem when drying particle blends is to ensure good mixing. This is complicated by the inherent desire for the film to stratify during the drying process. Such an occurrence will negate any gain achieved from blending particle properties.

A different type of particle blending is discussed by Qiao *et al* [131]. These authors mixed an aqueous latex dispersion with different amounts of halloysite nanotubes. The

observation was that the cracking propensity decreased upon nanotube addition and that the nanotubes were well dispersed within the film. The reason for the lack of cracks is difficult to state definitively. The authors speculate that the increased porosity in the composite films means the latex particles are held apart a larger amount and consequently the capillary pressure is reduced. This then reduces the driving force for cracking.

4.6.6. Supercritical drying. If capillary stresses can be eliminated during drying then the driving force for cracking is removed. The curvature of the air–water interface is caused by the presence of particles and is unavoidable for a colloidal film. The other parameter that can potentially be altered is the surface tension, and at the critical point of the solvent the surface tension becomes zero. Therefore, if the drying process involves going from the liquid state, through the supercritical regime and into the gas state then, at least conceptually, such a process will negate the possibility of cracking. The critical point for water is 374 °C and 218 atm, which are unlikely conditions to be used to dry colloidal films, and if one did, other stresses are likely to be introduced. Carbon dioxide has a critical point of 31 °C and 73 atm and it is feasible to, at least imagine, drying a film from such a solvent. Whilst supercritical drying has been shown by Bellet and Canham [132] for drying of porous silica materials, the author is not aware of any reports of such drying for colloidal films.

5. Evaporation

Evaporation drives the flows and consequently pattern formation in drying films. Understanding and predicting the rate of evaporation from any geometry of drop or film is the crucial first step in any model of film drying. There are a number of complications that need to be considered. The film geometry and specifically the curvature near the film edge can lead to a large increase in the local evaporation rate. The presence of particles within the film leads to a phase change at close packing and this could affect the evaporation rate. Within the film the capillary pressure builds up during evaporation, with a maximum value that can be supported. The magnitude of this capillary pressure, when compared with the cavitation pressure of water, could be argued to point towards cavitation, although paint films are not observed to spontaneously explode upon drying. These areas are considered in this section.

5.1. Film pinning

As a film, or droplet, of pure fluid dries there are two possible scenarios with regards the film dimensions: the film may either pin or recede. If the substrate is rough and the liquid sufficiently wetting the film will pin at its original position. This results in a reducing contact angle at the edge during evaporation. In this scenario the contact area between the film and the substrate remains constant. Alternatively, if the edge of the film is not pinned, then it recedes as drying proceeds. In this case the film is observed to display a constant contact angle [133, 134]. For particulate films a pinning motion is

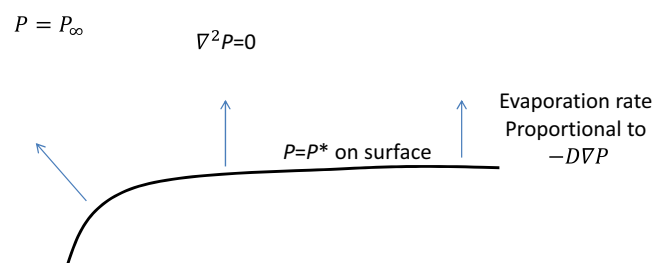


Figure 16. The evaporative flux from a drying film into stagnant air is determined by diffusion of water vapour. The vapour pressure, P , is determined by the solution of Laplace's equation subject to boundary conditions of the vapour pressure being the saturated vapour pressure at the surface of the film and the vapour pressure being at ambient conditions at large distances away. D is the diffusion coefficient of water vapour in air and P^* is the saturated vapour pressure of water.

generally observed. This is likely to be because the solidified regions of the film increase the shear stress between the film and substrate at the edge of the film and so hold the edge at its original position. The experiment where a film is cast on a pool of mercury negates any film pinning [73, 75]. In this case the film is observed to not crack (again due to relaxation of lateral stresses) and, although the articles do not explicitly state, it seems likely that horizontal drying fronts will be minimized.

5.2. Rate of evaporation

As pointed out by numerous papers [135–137] evaporation is a diffusion controlled process: the gaseous region immediately above any liquid water is saturated with water vapour at the saturated vapour pressure. The timescale for equilibration of the saturated vapour layer is given by Popov [135] as many orders of magnitude shorter than any evaporation time. In addition, as shown by Hu and Larson [138], the time taken for the vapour concentration profile to change in response to any change in droplet shape is also much less than the droplet evaporation time. Consequently evaporation from a film may be considered as a quasi-static problem.

5.3. Large films

In this section we consider the case of a large expanse of fluid and show that in most cases the evaporation rate can be taken as a constant value per unit area. The magnitude of the evaporation is then only a function of the humidity and temperature. The case of droplets is slightly different with the geometry of the air–water interface being relevant and this scenario is considered in section 5.4.

5.3.1. Evaporation into stagnant air. The simplest problem to consider is of an evaporating film in stagnant air. A sketch to show how the vapour concentration and hence the evaporation rate can be determined is shown in figure 16. The local water vapour pressure is given by solution to the diffusion equation, subject to boundary conditions at large distances and at the film edge. The evaporative flux is then given by the gradient in the vapour pressure at the droplet surface.

Note that we are using the vapour pressure instead of water vapour concentration and are assuming an ideal gas relation between the two parameters. At atmospheric pressure and room temperature this is a reasonable assumption.

The easiest geometry to consider is an infinite flat expanse of fluid. In this case the evaporation rate is uniform across the film and is a function of temperature and relative humidity only. The evaporation rate can be easily determined through mass loss experiments and expressed as a mass per unit area per unit time. Alternatively the mass loss can be expressed as a volume of liquid water, and the evaporation rate then becomes a velocity, which corresponds to the rate of height loss of a film [139]. For evaporation at 22 °C, with a relative humidity of about 50% the evaporation rate of pure water is found to be about 0.3 cm per day [45].

The presence of an edge to the film complicates the boundary condition, and the film geometry then affects the evaporation rate. For the geometry shown in figure 16 the vapour pressure field can be easily calculated and consequently the evaporation rate predicted. It is found that the local evaporation rate is higher at the edge of the film, compared with the flat region of the film. In addition the degree of curvature at the edge affects the difference in the evaporation rate. There are many reasons why this non-uniform evaporation rate is typically ignored: the first is that for a large film the edge region only comprises a small portion of the film and so any extra evaporation is small when compared to the total mass loss. In addition the experimental observation of drying fronts have been successfully predicted using a uniform evaporation rate and so there has been no need to incorporate the complication into models [35, 139]. Also the film shape is dynamic and so to calculate the evaporation rate at each time step is a laborious process and the solution is then only valid for each particular initial condition. However, the main reason why the extra edge evaporation is typically ignored is expanded on in section 5.3.2. Any air flow over the film will typically cause the evaporation rate to be uniform across the film anyway.

5.3.2. Evaporation into flowing air. As intuitively expected, if the air surrounding the drying film is flowing then evaporation is enhanced. This is demonstrated experimentally by Croll [45] and is common experience in everyday life. Whilst conceptually simple, the flow of air will include a convection term in the conservation equation for water vapour. Consequently the equation to determine the water vapour pressure, P , will become $D\nabla^2 P - \mathbf{u} \cdot \nabla P = 0$, where D is the diffusion coefficient of water vapour in air and \mathbf{u} is the local air velocity. This can be a difficult problem to solve with the air flow needing to be solved to provide \mathbf{u} , which can then be included in the water conservation expression.

As an example it is intuitive to examine the simplest possible problem where the air velocity is spatially uniform and only in the direction directly across the film. The relative magnitudes of convection and diffusion are expressed in the Peclet number (LU/D), where L is the characteristic horizontal length scale for the film. If the convective flux is sufficiently large, such that $Pe \gg 1$, then diffusive effects can be ignored. In this case the gradient in vapour pressure

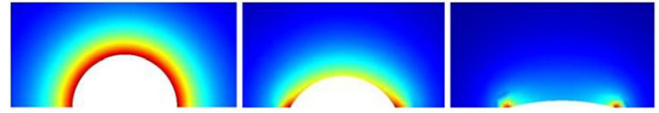


Figure 17. Numerical solution for evaporative flux from a droplet. Images show vertical cut through the centre of a droplet and red indicates a high flux and blue indicates a low flux. For a 90° contact angle the evaporative flux is uniform across the drop whereas for lower contact angles enhanced evaporation is observed at the droplet edge. The numerical solution was created by Thomas Collins and David Gibney.

is small throughout the domain and the evaporation rate is constant across the drop. The physical reason is that if air flow over the drop is sufficient to remove evaporating molecules as soon as they pass into the gas phase, then the mass transfer is controlled by the ability of water molecules to pass into the gas phase and not the diffusion of water vapour away from the droplet. Interestingly if we take the diffusion coefficient of water vapour in air as $10^{-9} \text{ m}^2 \text{ s}^{-1}$ then, for a film with characteristic size 1 mm, a uniform evaporation profile would be expected for air-flow rates greater than 10^{-6} m s^{-1} , which is an air velocity of 2×10^{-6} miles per hour. Not many labs are able to restrict air flow to less than such a level, without very controlled conditions. This result suggests that most examples of drying films are likely to be subject to a uniform evaporation rate across their surface.

5.4. Evaporation of droplets

The physics of mass transfer for an evaporating droplet, is the same as for a large film, and is explained above in section 5.3. In the case of droplets a difference occurs because the edge region comprises more of the film and the simple flowing air argument, given above, is unlikely to relate to a small droplet, where the velocity field will be complex and not unidirectional. In addition as the characteristic size of the droplet decreases, the Peclet number decreases, and the importance of diffusion increases.

For an evaporating droplet, solution of the Laplace equation, and calculation of an evaporative flux is carried out by Hu and Larson [138]. They show numerical results of how a sessile droplet of pure water will evolve over time and demonstrate a divergent evaporative flux at the drop edge. Deegan *et al* [137] show that for a drop of radius P and contact angle θ the flux diverges at the edge with a functional form

$$\dot{E} (P - r)^{-\lambda}, \quad (2)$$

where λ is given by $\lambda = (\pi - 2\theta)/(2\pi - 2\theta)$. Deegan *et al* [137] give a physical explanation for the singularity as the curved surface increasing the probability of a gas molecule moving away from the liquid surface and not re-colliding. Popov [135] gives explicit solutions to the diffusion problem to calculate functional expressions for the evaporation rate. It should be noted that, physically, the singularity must be integrable, so that the total rate of mass loss is finite.

A numerical solution for the evaporative flux is shown in figure 17. This solution is obtained by solving the Laplace equation, subject to boundary conditions of the saturated

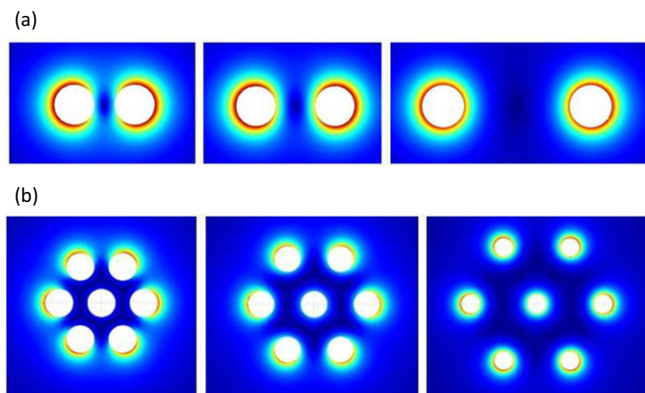


Figure 18. Numerical solution for evaporative flux from droplets arranged in different arrays. Images show droplets from above and red indicates a high flux and blue indicates a low flux. The numerical solution was created by Thomas Collins and David Gibney.

vapour at the drop edge and zero vapour at large distance. Once the vapour concentration field is obtained the flux is determined by plotting the gradient in the vapour concentration. The results are shown for three droplets with different contact angles. As can be seen, for a contact angle of 90° the flux is uniform across the droplet. As the contact angle decreases the enhanced edge evaporation becomes more pronounced.

As in the case of large films it is unlikely that the surrounding air is stagnant and so it is necessary to include a convective term in the water vapour conservation expression. This becomes a hard problem to solve. Numerical solutions are inevitable and the three phase contact line is especially hard to resolve. However it is conceptually simple to see how solutions can be formed.

The divergent evaporative flux has been incorporated in models for drying droplets by Fischer [140], with a range of functional forms for the evaporative flux used. The results showed that both enhanced evaporation at the droplet edge, and a uniform evaporation rate across the entire droplet, resulted in ring formation. Interestingly the (presumably unphysical) case of enhanced evaporation at the centre of the droplet resulted in the absence of ring formation in the drying drop. The different explanations for formation of ring deposits have been discussed in section 1.2.1.

5.4.1. Multiple droplets. When an array of droplets is deposited on a surface the vapour fields from different droplets will interact and hence the evaporation of a droplet will be affected by its neighbour. The effect is elegantly shown by Deegan [136], where two droplets drying side by side display a weakened accumulation of material in the region closest to the neighbouring drop. This issue is most important in applications such as inkjet printing where print densities of many hundreds of drops per square inch is common [141]. Figure 18 shows a numerical solution for the evaporation rate from drops arranged in different arrays. In figure 18(a), two droplets with a 90° contact angle are placed a short distance apart, and the effect that each has on the evaporation of the other is evident. Unsurprisingly, as the separation between droplets is increased the interaction reduces. Figure 18(b)

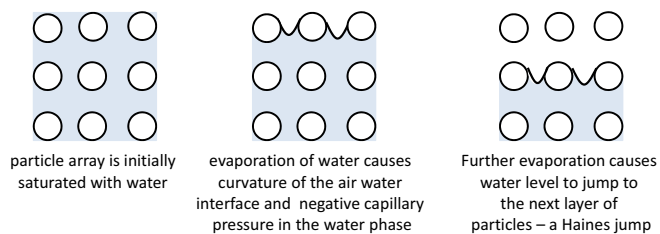


Figure 19. Sketch showing the process of a Haines jump. Once the capillary pressure reaches its maximum value the water recedes through the film at this pressure and hence at a constant curvature.

shows droplets arranged in a hexagonal array. The evaporation from the central drop is significantly reduced in comparison with the edge droplets and again increasing the separation between the droplets minimizes the interaction.

5.5. Effect of particle volume fraction

The saturated vapour pressure of water is thermodynamically determined, such that the chemical potential of water in the vapour phase exactly balances the chemical potential of liquid water. The presence of solutes, or particles, in the liquid phase will affect the water chemical potential and consequently the saturated vapour pressure and evaporation rate. Experimental evidence is that any such effect is small, with the evaporation rate from a dispersion proceeding at a very similar rate to the case of pure water. Croll [44, 45] reports evaporation from a dispersion of commercial latex at 85% of the rate for pure water, although Croll ascribes the slower mass transfer to a reduced rate of heat transfer to the paint, resulting in an increase in evaporative cooling. Routh and Russel [139] show that the effect of particle volume fraction on the water vapour pressure is irrelevant until the particles undergo a phase transition and the osmotic pressure diverges. It is usual, and seemingly reasonable, to ignore any reduction in evaporation rate as particles consolidate within a film.

5.6. Control of humidity

For an infinite flat expanse of fluid the evaporation rate can be written as $\dot{E} = k^+(\mathcal{H}^* - \mathcal{H})$, where k^+ is a mass transfer coefficient, \mathcal{H}^* is the saturated humidity and \mathcal{H} is the humidity. The mass transfer coefficient and saturated humidity are functions of temperature, whereas the local humidity \mathcal{H} can be controlled by the amount of water vapour present in the air.

A standard way to experimentally control the humidity, within a drying chamber, is to use saturated salt solutions. Different salts produce different relative humidities, with the specific value being a weak function of temperature. There are tabulated values of the relative humidity that result from different salts [142, 143] and experimentally it is simple to set-up such a humidity chamber.

5.7. Capillary pressure

An interesting aside concerns how water recedes into a drying film. Consider the simple case of an infinite expanse of film evaporating uniformly, as sketched in figure 19. As the

particles consolidate, water is held at the top surface and, upon further evaporation, the water pressure decreases due to the curvature of the air–water interface. At some point the capillary pressure reaches its maximum value and the water then recedes into the film. To keep the pressure at its maximum capillary value, the curvature of the air–water interface must remain set and so the interface must ‘jump’ to the next available pore throat. This is called a Haines jump [144]. Such bursting motion is well known in the soil mechanics literature and has been characterized by electric field bursts [145], although such jumping motion seems to be less well recognized by the drying film community. A sketch showing the steps associated with such jumps is shown in figure 19.

The magnitude of the capillary pressure in the drying film brings in other interesting considerations. Geometrically the maximum achievable value for capillary pressure is $A\gamma/R$ where A is a constant around 5 [31]. For particles with a radius of 10 nm, in water with a surface tension of 73 mN m^{-1} , the capillary pressure is calculated as 36.5 MPa. This is a negative pressure in the water phase and at a certain magnitude cavitation would be expected to occur. The value for the cavitation pressure is a function of temperature and subject to debate, but a value around 20 MPa at 20°C seems reasonable [146]. Therefore drying films with very small particles would be expected to experience water cavitation, yet films have never been observed to explode upon drying! A similar issue arises within trees, where the capillary pressure is used to suck water up large heights [147]. Whether confinement within small pores, or the inability to nucleate sufficiently sized bubbles stops the cavitation is, as far as the author is aware, an open issue.

6. Thin film fluid mechanics

The main parameter of interest for a drying film is how the film height varies with position and time. This is determined by the fluid mechanics of the film and how the fluid flows in response to the evaporative loss of material. For thin layers of fluid, the flow is conveniently described using lubrication theory, which greatly simplifies the governing equations. Two comprehensive reviews of the fluid mechanics surrounding lubrication theory are the work of Oron *et al* [148] and Craster and Matar [149]. We do not propose to go into the depth of these reviews here, but merely highlight the most important parameters. The issues with regards drying colloidal dispersions tend to be whether lubrication theory is applicable, the effect of particles on the resulting flow, the effect of surfactants, which may well be initially adsorbed onto the particles, and prediction of flow patterns in the drying films.

6.1. Lubrication theory

The full Navier–Stokes equations apply to any Newtonian fluid. For flows where the vertical length scale is much smaller than the horizontal length, over which the film evolves, the mathematics may be greatly simplified by the lubrication approximation. In a thin film it is natural to scale vertical distances with the initial film height, H . Depending on the

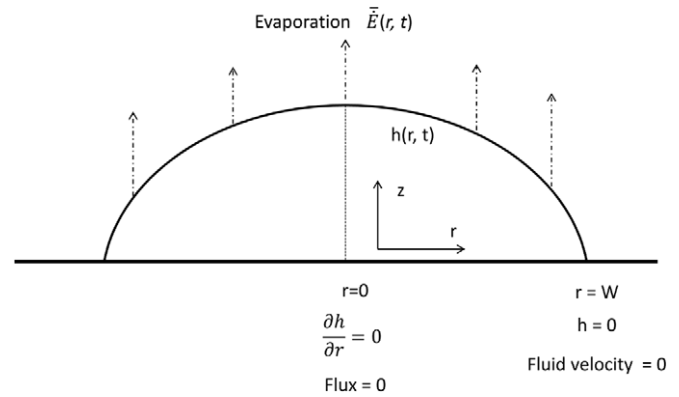


Figure 20. Sketch defining the geometry of an axisymmetric drop on a substrate subject to evaporation.

problem specifics there may be a natural horizontal length scale, such as the drop radius. Alternatively the film evolution may be seen to occur over much larger horizontal distances. Referring to the characteristic horizontal distance as L one can scale the Navier–Stokes equations. The lubrication approximation assumes that the vertical length scale is much smaller than the horizontal one and also that the inertial terms are negligible [150]. Mathematically this is expressed as $H^2/L^2 \ll 1$ and also $(H^2/L^2)Re \ll 1$, where Re is the Reynolds number of the flow.

Following Fischer [140] we consider the case of an axisymmetric drop of radius W , in cylindrical coordinates with radial coordinate r and vertical coordinate z , as sketched in figure 20. The velocity in the radial direction is u and in the vertical direction is v . The characteristic horizontal velocity for the flow is given by the viscous velocity, $U_c = \mu/\rho H$ and the characteristic pressure is $\mu U_c L/H^2$, where μ is the fluid viscosity and ρ the density. Upon scaling and neglecting the terms of order H^2/L^2 the Navier–Stokes and continuity equations provide

$$\frac{\partial p}{\partial z} = 0 \quad (3)$$

$$\frac{\partial p}{\partial r} = \frac{\partial^2 u}{\partial z^2} \quad (4)$$

$$\frac{1}{r} \frac{1}{\partial r} (ru) + \frac{\partial v}{\partial z} = 0. \quad (5)$$

As seen from equation (3), within the lubrication approximation, the pressure is found to be uniform vertically across the film. This means that the pressure at the top surface determines the resulting flows and it is determined by the surface tension and curvature of the top surface. The pressure follows as

$$p = -\frac{1}{Ca} \frac{1}{r} \frac{\partial}{\partial r} \left(r \frac{\partial h}{\partial r} \right), \quad (6)$$

where the dimensionless number Ca is called the capillary number and is given by $Ca = \mu^2 L^3/(H^4 \rho \gamma)$, with γ the surface tension of the fluid. Consequently the entire flow is determined by the capillary number, which quantifies the relative importance of viscous and surface tension forces. For large capillary numbers the surface tension is small and the film will readily flow. For small capillary numbers the surface

tension is dominant and rounded shapes in the film will be observed.

The evaporation rate is taken as spatially varying and, upon scaling with the characteristic vertical velocity ($L\mu/\rho H^2$), it is written as $\bar{E}(r, t)$. A mass balance on the fluid at the top surface, subject to no slip at the bottom interface and zero shear at the top surface provides a partial differential equation for the droplet height, h as

$$\frac{\partial h}{\partial t} = -\frac{1}{3Ca} \frac{1}{r} \frac{\partial}{\partial r} \left[rh^3 \frac{\partial}{\partial r} \left(\frac{\partial^2 h}{\partial r^2} + \frac{1}{r} \frac{\partial h}{\partial r} \right) \right] - \bar{E}(r, t). \quad (7)$$

Equation (7) is valid for situations where the surface tension and viscosity are constant. When this is not the case it is relatively simple to include correction terms. There are numerous examples of solutions to equation (7) and Fischer [140] examines many different evaporation profiles.

The main advantage of the lubrication approximation is that it greatly simplifies the Navier–Stokes equations and provides a partial differential equation for the film height. In situations where the lubrication approximation is not valid, the numerical issue becomes one of tracking the free top boundary and allowing a vertical variation in pressure through the film [151]. This is, computationally, a far harder problem to solve and the literature is far smaller, when compared to lubrication theory.

6.2. Effect of volume fraction

Inclusion of particles in the drying droplet provides a conservation equation for particle volume fraction. Again following Fischer [140] and using the same geometry as described in section 6.1 the conservation expression for particle volume fraction becomes

$$\frac{\partial h\phi}{\partial t} = -\frac{1}{3Ca} \frac{1}{r} \frac{\partial}{\partial r} \left[rh^3 \frac{\partial}{\partial r} \left(\frac{\partial^2 h}{\partial r^2} + \frac{1}{r} \frac{\partial h}{\partial r} \right) \phi \right]. \quad (8)$$

One inevitable complication is that as evaporation proceeds, the dispersion viscosity increases. There are numerous expressions for the low shear viscosity of a dispersion as a function of volume fraction, with the Krieger correlation being perhaps the most common [1]. Within the lubrication approximation the vertical profile of volume fraction is determined by the Peclet number, as discussed in section 3. Gundabala and Routh [152] solved the lubrication equations for the case of an added surfactant with the particle volume fraction assumed to be uniform across the film thickness. If the volume fraction is not uniform vertically and the viscosity is allowed to vary with volume fraction, it is still possible to solve for the velocity field, as a function of position, although the expressions become more complex. This problem was tackled by Yiantsios and Higgins [153], who look at the Marangoni flows due to evaporative cooling, whilst retaining the 2D nature of the particle concentration field.

6.3. Effect of surfactant

The pressure in the film is a result of the film curvature and the local surface tension. Any accumulation of surfactant at the

air–liquid interface will lower the surface tension and cause a flow away from such a region. The flow is observed to occur via fingers rather than in a simple radial fashion [154]. Such situations, which are driven by gradients in surface tension are termed Marangoni flows [155].

With regards drying colloidal dispersions, surfactants are often added to aid colloidal stability and the possibility of Marangoni induced flows therefore arises. The surfactant will be bound to the particles and if merely physically adsorbed an adsorption isotherm will determine the amount in the serum. As evaporation concentrates the dispersion, the surfactant in solution will inevitably concentrate and as particles consolidate they may well displace further surfactant. Such a system is described by Harris and Lewis [17] who observed pattern formation when drying suspensions of silica particles in ethanol. As is intuitively expected, Harris and Lewis observed that if the initial dispersion volume fraction was above a critical value, the Marangoni flows were suppressed. Gundabala *et al* [61] modelled the stability of thin films where the surfactant is desorbed from particles as they consolidate. This produced an unstable system and using tapping mode AFM Gundabala *et al* observed the predicted undulations in the surface of a pressure sensitive adhesive system.

The model of Gundabala *et al* [61] demonstrates how complex a system can become. The surface tension reduction is determined by the surfactant concentration at the air–liquid interface. This is coupled to the surfactant concentration in the fluid, through an adsorption isotherm, and this concentration couples with the local particle volume fraction via a separate adsorption isotherm. The complexity means that there are many possible directions for future research. The surface chemistry of the particles determining the desorption rate of surfactant and this leading into the observed flow instability being an attractive area for study.

6.4. Effect of temperature

Just as variations in surfactant concentration can lead to a surface tension gradient, any non-uniform temperature will also affect the film. The simplest case to analyse is when the bottom of the film is heated and the top surface remains cooler. Such a scenario would arise when a drying film is observed under a microscope, with the inevitable lamp heating, causing a temperature gradient.

The experimental observation is of the formation of undulations in the film surface into a hexagonal cellular structure, called Bénard cells. The size of the cells is a little larger than the film thickness. One explanation could be for the reduced density of hot fluid, resulting in a buoyancy driven flow from the bottom surface to the top, and hence convective rolls. The prediction however is for such flows to only occur in thicker films and it is well established that Bénard cells are due to variations in surface tension [156, 157]. The physical explanation is that when the film experiences a height undulation the thicker part of the film will have a cooler top surface and therefore a higher surface tension, pulling fluid into this region and therefore exacerbating the height undulation. This is sketched in figure 21.

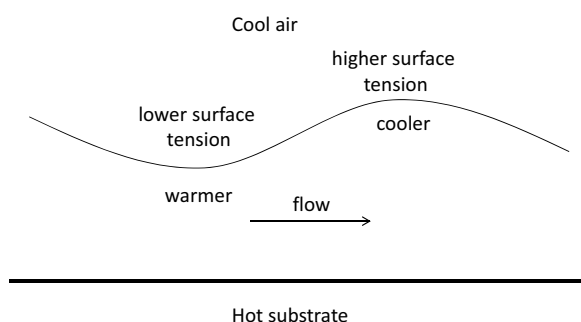


Figure 21. Physical basis for formation of Bénard cells. Thicker regions of the film are cooler and therefore have a higher surface tension. This results in flow from the thin to thick regions of the film.

The mathematical explanation is due to Pearson [158], who demonstrated that a linear stability analysis predicted an instability when surface tension variations with temperature are sufficient to overcome viscous resistance. Pearson also makes the comment that evaporative cooling should cause the same effect and this is used by Yiantsios and Higgins [153] to predict natural undulations in evaporating films.

6.5. Boundary conditions

The partial differential equation for film height, equation (7) requires four boundary conditions. The simplest case involves a droplet of pure fluid pinned at its original radius and this scenario is sketched in figure 20. At the centre of the drop, $r = 0$, symmetry dictates that the film profile is flat, $(\partial h / \partial r) = 0$. In addition zero flux of material across the centre line dictates a zero fluid velocity. The other two boundary conditions are at the edge of the drop. The first is that the film height is pinned at $h = 0$. The final condition is naturally a fixed contact angle, although as discussed by Fischer this can change with time as fluid becomes depleted [140]. In addition, upon scaling, within the lubrication approximation this is found to be $(\partial h / \partial r) \gg 1$. It is possible to demonstrate that an equivalent boundary condition is that the fluid velocity is small at the edge of the drop and this has been used successfully [139].

Once a packed region of consolidated particles forms at the edge of the film the boundary condition must change to accommodate this. The boundary condition at the point of the fluid solid transition becomes the film height being fixed and the flux of solvent through the front balancing the total evaporation from the consolidated region. A number of models have been created with evaporative profiles from the consolidated region varying from continued evaporation [139] through to no evaporation at all from the consolidated particles [159].

6.6. Prediction of flow patterns

Prediction of the flow profiles within drying films or droplets is the subject of many studies. Fischer [140] examined numerically how the capillary number affects the resulting flows. For small capillary numbers, which represents strong surface tension, the droplet shape remained smooth. For weaker surface tension the film profile displayed more

undulations and Fischer reports a tendency for the film to depin from the edge. Fischer also examined the effect of different evaporative models on the flow profiles. He used different scenarios ranging from a flat evaporation profile through to enhanced evaporation at either the edge, or the centre. When evaporation was enhanced at the centre the edge drying was minimized with the final film profile appearing uniform. Other evaporation profiles lead to accumulation of material in a ring at the edge of the film.

A similar study is carried out by Okuzono *et al* [159]. Their work examines a polymer solution, although the gelation above a critical concentration allows a direct analogy to the particulate system. The evaporation rate is taken as a constant although the paper notes that this is an approximation and solution of the diffusion equation in the gas phase would allow prediction of the evaporation rate. A further paper from the same group [160] demonstrates how an array of droplets causes the surrounding air to have a complex water vapour concentration field and the subsequent effect on droplet evaporation affects the final droplet profile.

Wang and Evans [161] report on drying of droplets containing two or three different particle types. Whilst they do not explicitly solve any flow equations they ascribe the various final droplet profiles observations to a combination of the horizontal drying front and Marangoni flows due to stabilising surfactant. In addition to different droplet morphologies they also observe stratification of the different components during drying.

7. Experimental techniques to follow drying in thin films

In this section we describe a number of experimental techniques that have been used to examine drying colloidal films. We do not aim to give exhaustive experimental details, rather the aim is to give interested readers knowledge as to available techniques and the information that can be obtained. We concentrate here on the techniques themselves rather than any specific findings, which are described elsewhere in this article.

7.1. Microscopy

The simplest way to follow a drying film is to look at it. Many of the transitions of interest occur over centimeter length scales and as such are readily followed optically. Other transitions can occur on the particle length scale and so electron microscopes provide the necessary resolution.

7.1.1. Optical microscopy. As would be expected there are numerous studies of drying colloidal films using optical microscopy. Weon and Je [162] followed the motion of microsphere tracer particles during the drying process to elucidate flow directions. Whilst simple to perform such experiments, care must be taken to ensure any heating, through illumination, does not cause flow and hence artefacts.

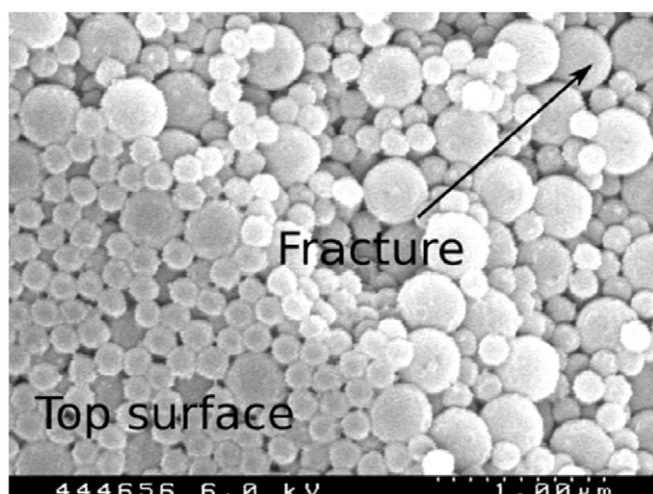


Figure 22. Typical cryo-SEM image showing a cross-section through a film. In this case the film contains two types of particle and the technique allows visualization of the arrangement of particles.

7.1.2. Freeze-fracture SEM. To enable imaging of particle arrangement across the film depth, it is necessary to fracture the film. One elegant way to do this is freeze-fracture SEM, (often also called cryo-SEM), where the film is frozen in a cryogen such as liquid nitrogen, fractured, and then imaged on a cold stage. This technique has been extensively used in biology [163]. For drying colloidal films the major advantage is easy control over the drying time allowed, before the sample is frozen, and the direct observation of the particle arrangement. Some beautiful images showing particle arrangements within the drying coating have been obtained. Examples can be found in Luo *et al* [59, 164] and Ma *et al* [38]. The major artefacts that can occur during the experiment are ice crystal formation, as discussed by Luo *et al* [164] and the deformation of particles into ‘elongated protuberances’ [38], resulting in the fracture surface not being a clean cut through the sample. A typical cryo-SEM image is shown in figure 22 and the arrangement of particles is easily observed.

7.1.3. Environmental SEM. Conventional SEM operates under a high vacuum and consequently cannot be used to image wet systems. Environmental SEM (ESEM) allows samples to be held at pressures of up to 1/20th of an atmosphere. This allows wet samples to be imaged in the presence of water vapour and hence still in their wet state [165].

Examples of the use of ESEM on drying colloidal dispersions include the work of Keddie *et al* [166, 167] who studied film formation and Dragnevski *et al* [168] who looked at crack propagation. The latter demonstrated the ability to cycle humidity in the sample chamber, through the use of temperature, and consequently to dry and then re-wet the film. Figure 23 is taken from Dragnevski *et al* [168] and shows a crack propagating through a wet film. This demonstrates the power of ESEM in being able to image the drying process in-situ. Along with conventional SEM, the biggest drawback with ESEM remains that the image is only from the top surface of the film.

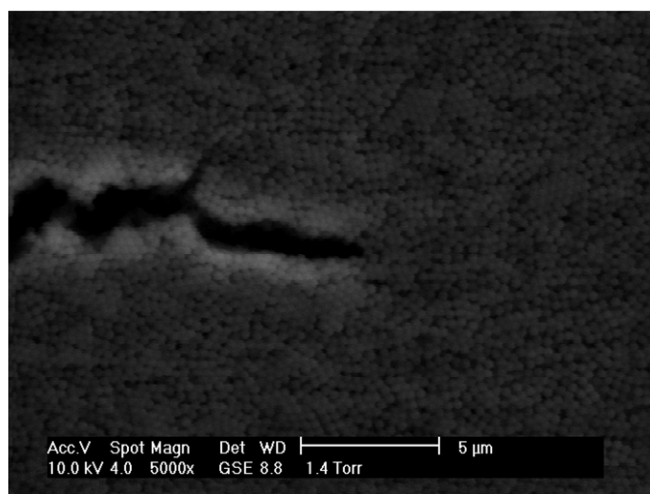


Figure 23. ESEM image of a crack propagating through a drying film. The individual particles, which are 300 nm in diameter can be seen. Image reprinted with permission from [168]. Copyright (2010) American Chemical Society.

7.1.4. Atomic force microscopy. AFM samples a surface with a fine tip, allowing images of individual particles on the surface of a drying film. It has been used to measure the composition at the top surface in bi-disperse particle mixtures [56]. Goehring *et al* [105] used AFM to image a crack as it propagated through a drying film. The relative motion of particles in the vicinity of the crack tip allowed the local plasticity to be demonstrated. In addition, on larger length scales, height profiles can be obtained in films, over areas of about $25 \mu\text{m}^2$. This is shown by Tzitzinou *et al* [169] on hard acrylic latex films. For softer films, where the tip can cause damage to the film and consequently affect the height measurement, Mallegol *et al* [170] show how tapping mode AFM can sample the film surface and obtain a height image. For the soft films used by Mallegol *et al* the phase response of the tip to the driving frequency gave information about the adhesive properties of the surface and hence the composition. This technique was also used by Lei *et al* [60].

Figure 24 demonstrates the range of information available from AFM imaging on drying films. Figure 24(a) shows the top surface of a film that contained two different particle sizes. The different particles are easily distinguished and hence the relative amounts of the two components can be determined. On a larger length scale, figure 24(b) shows (i) topological and (ii) phase images from the top surface of a pressure sensitive adhesive, using tapping mode. The topological image shows a depression in the film surface and the phase image shows that the film is stickier in the regions of depression. Lei *et al* [60] attributed this to an accumulation of surfactant in the regions of the film with the depressed surface. Figure 24(c) shows how complex surface topologies can be detected using AFM.

7.2. Following water in a drying film

During the drying process, water is the component that is often of most interest. Tracking water allows the particle volume fraction to be inferred and it also elucidates the pathways for

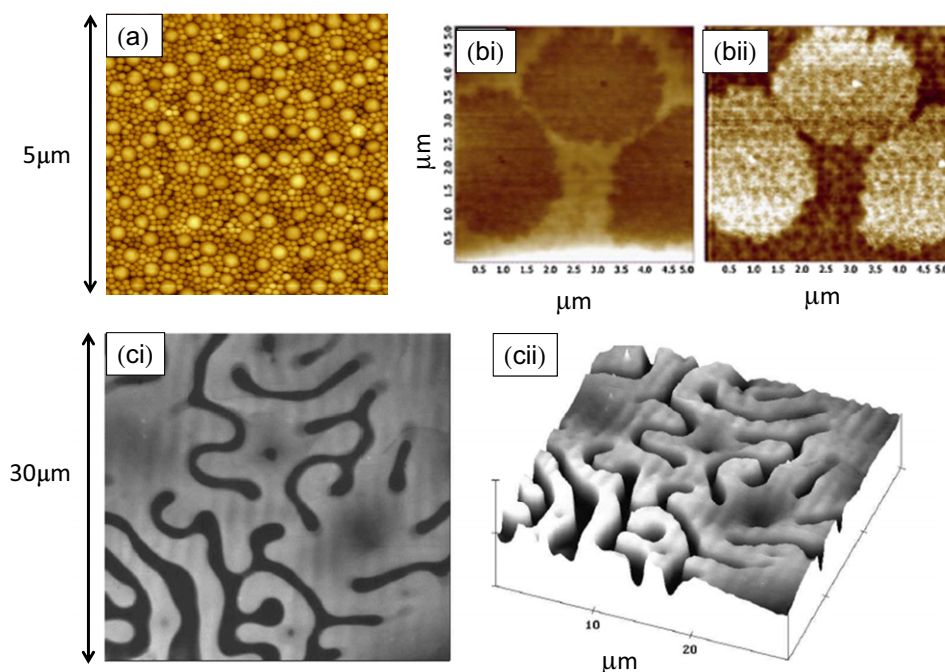


Figure 24. Examples of information obtainable using an AFM. (a) demonstrates the ability to distinguish different particles at the top of a film. (bi) shows a topographical image from the surface of a pressure sensitive adhesive (bii) shows the phase image and demonstrates that the surfactant is present in the depressions in the film surface. (ci) shows the top image of a silicone/polyester substrate and (cii) shows a 3D representation of the surface. (a) reprinted with permission from [55]. Copyright (2012) American Chemical Society. (b) reproduced from [60] with permission from Elsevier and (c) reproduced from [170] with permission from Taylor and Francis Ltd.

evaporation. To track water in a film that is only tens of micrometres thick, and evaporating over a period of an hour, is not an easy task. The suitable techniques are either MRI or a specialized spectroscopy.

7.2.1. 2D MRI. Exploiting MRI in two dimensions allows the water content in drying films to be followed laterally as well as vertically. Salamanca *et al* [33] followed the lateral drying of films and determined the time that water receded from the edge. A review of the use of MRI in a range of physical processes is given by Mantle and Sederman [171].

7.2.2. GarField NMR imaging. MRI relies on a gradient in magnetic field strength. Instead of using magnets with different strengths, the GarField technique relies on the shape of a permanent magnet, to produce a well-defined magnetic field strength gradient in the vertical direction. This allows the relative amount of mobile protons to be measured vertically through the film, with a resolution of about $5\ \mu\text{m}$ [172]. The technique has been used extensively by the group at Surrey to examine uniformity of drying [64] and even cross-linking reactions during the drying process [66].

Representative results from a GarField experiment on a drying film are shown in figure 25. The magnetization on the vertical axis is proportional to mobile protons and, for this aqueous dispersion of hard latex particles, is proportional to water concentration. Figure 25 shows results from an experiment on a drying film. Figure 25(a) is for a Peclet number of 0.2, achieved with very slow drying. As can be seen the film thickness decreases with time as evaporation proceeds.

The magnetization profiles are however flat across the film thickness and this demonstrates a uniform water concentration through the film. As expected, as time proceeds, the water concentration then decreases but remains spatially uniform. Figure 25(b) is for a Peclet number of 17 and is achieved with faster drying rates. In this scenario the concentration of water at the top surface of the film is below the bulk value and this is evidence for formation of a particulate skin layer at the top of the film.

7.2.3. Laser-scanning coherent anti-Stokes Raman spectroscopy. The ability to detect water with a microscope was demonstrated, by Dufresne *et al* [99, 100], using laser-scanning coherent anti-Stokes Raman spectroscopy (CARS). This technique detects the OH stretch of a water molecule, with images appearing bright when water is present and dark otherwise. Dufresne *et al* were able to demonstrate that compaction fronts are indeed a region of increased particle concentration, although still wet. They also demonstrated that cracks form in wet material, although are devoid of water within the crack itself.

7.2.4. Inverse micro-Raman spectroscopy. Using confocal Raman spectroscopy with an inverse microscope allows the water content to be determined with a spatial resolution of about $2\text{--}3\ \mu\text{m}$ [173, 174]. A group at Karlsruhe University has developed and used the technique to follow both horizontal drying fronts and the vertical drying profiles in polymer films. As well as following the drying step Ludwig *et al* [173] followed the subsequent film formation of polymer particles after compaction of the film.

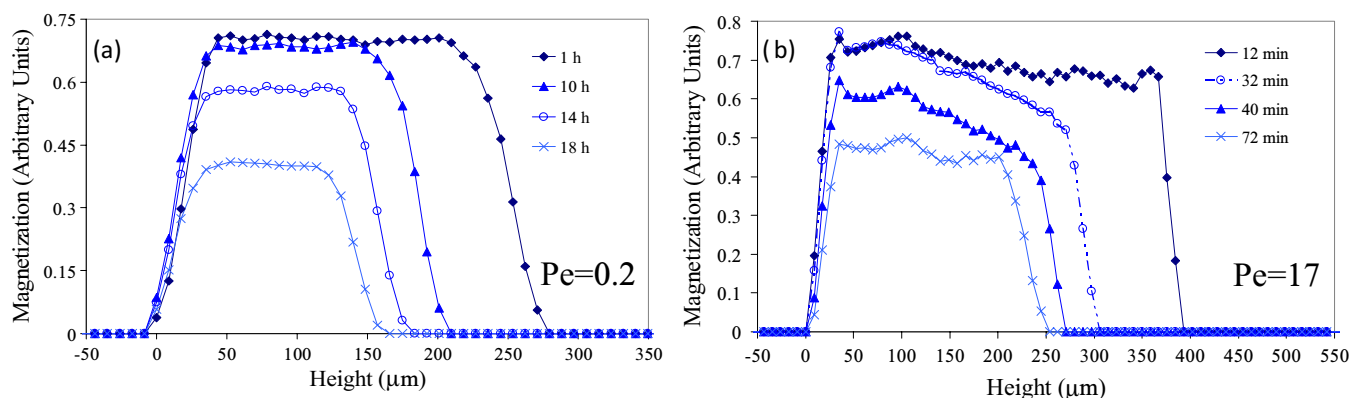


Figure 25. Representative results from a GarField experiment on a drying film. (a) For slow drying (low Peclet number) the water profile across the film is seen to be uniform. (b) for faster drying (high Peclet number) non-uniform water profiles are observed. Image courtesy of Professor Joe Keddie, University of Surrey.

Arnold *et al* [175,176] report the use of confocal Raman spectroscopy to determine the local concentration of sodium dodecyl sulfate (SDS) surfactant, at differing depths and lateral positions, within a dry latex film. The technique provides a resolution of about $2\mu\text{m}$ and Arnold *et al* demonstrated a surprising heterogeneity in surfactant concentration throughout the film.

The advantage of any spectroscopic technique, such as CARS and inverse micro-Raman spectroscopy (IMRS), is the simplicity of using a microscope to examine the drying film. The disadvantage is the necessity for light to be able to penetrate the sample. For many dispersions containing, say 200 nm , particles the dispersion will be too opaque for any optical technique.

7.3. Following stress build-up in a film

During the drying process, the stress within the film determines the propensity of cracking, and also any deformation of constituent particles. The network stress is a direct consequence of the capillary pressure in the film. Another, analogous, way to view the stress development is that the film is free to consolidate normal to the substrate, but is confined laterally. This confinement results in the film being stressed [177]. To measure this stress a number of techniques have been developed, and we discuss these here.

7.3.1. Beam bending. The most popular method for measuring the stress in a drying film is beam bending. The concept is simple, with a cantilever beam having the film placed upon it. On drying the film wishes to contract and this imparts a compressive stress onto the beam, which bends in response. Detecting the deflection of the beam allows the magnitude of the stress to be determined. The first use of beam bending for drying films was reported by Petersen *et al* [39].

A typical stress profile is shown in figure 26. The profile shows a build-up of stress followed by a rapid decline at the onset of cracking, as described by Tirumkudulu and Russel [40]. The technique has many advantages in that it is relatively simple to change the temperature and humidity, by placing the film within a drying chamber [41, 178, 179]. There have been

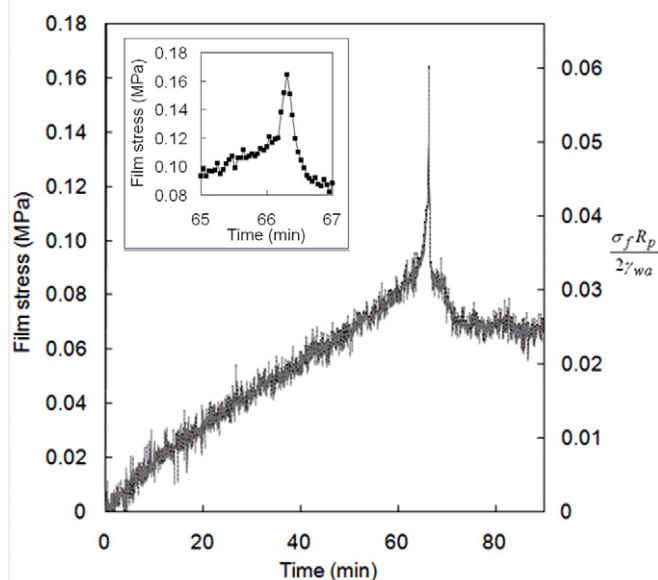


Figure 26. Typical stress profile from a beam bending experiment. The stress builds up and the sudden drop in stress is indicative of a crack forming and relieving the stress. Figure reproduced from [42] with permission from Elsevier.

numerous studies reporting the effect of particle mechanical response [41], particle size and film thickness [42].

The main disadvantage of beam bending is that it provides a single value for the stress across the entire film, whilst drying models all predict a spatial variation. Irrespective of this limitation, beam bending has become a well-accepted method of stress determination.

7.3.2. Membrane bending. In an attempt to overcome the spatial resolution issue, inherent with beam bending, von der Ehe and Johannsmann developed membrane bending [180]. This technique again relies on a stressed film pulling on the substrate causing a deflection. In this case the substrate is a flexible membrane and the deformation field is determined by placing an array of dots on the membrane surface. Any deformation results in distortion of the dots and this is picked up with a digital camera. The deformation field is resolved

to a resolution of 0.66 mm and consequently the stress field is spatially resolved.

The technique has been successfully employed by Konig *et al* [181, 182]. The work demonstrated the large build-up of stress locally around the drying front and also how the stress in the film locally fluctuated in response to variable evaporation rates. In addition films were observed to relax, after a drying front had passed, and experience a dilational stress. This information is only available from a spatially resolved stress measurement.

7.3.3. Traction force microscopy. A different way to obtain spatially resolved stress information is reported by Xu *et al* [183]. Traction force microscopy relies on the elastic deformation of a compliant substrate and has been used to follow the stress distribution around a crack. The difference from membrane bending is that the deformation of the substrate is larger, so that the elasticity equations for the substrate are solved in full, rather than linearized. The technique has been applied to a simple droplet, examining the stress balance at the edge [184], as well as drying stresses in skin [185].

7.3.4. Newton's rings. Another way to measure deformation of a substrate is through interference of reflected light. This is called Newton's Rings and can be used to measure the stress in a film deposited on a fairly rigid substrate [186]. The method has been employed by Clegg *et al* to follow the stress through the compaction front of a drying film.

7.4. Measuring film height

For a dried film, the final height profile is often the most important factor and there are a number of techniques for measuring the profile. For small areas AFM, as discussed in section 7.1.4, will provide the surface topology. However for larger areas different techniques are needed to obtain data within a reasonable time-frame. In addition there are a few techniques that can provide the film height profile during the drying process.

7.4.1. Profilometry. The simplest method to determine a film height profile is through profilometry. A common type is contact profilometry, where a needle is dragged over the film surface, producing a profile of the film surface [152]. To produce absolute thickness data it is necessary to somehow place the needle onto the substrate, either through removing the film in some region, or having a region that is not cast. One possible disadvantage of contact profilometry occurs if the film is sufficiently weak, so that the needle causes damage and changes the film height profile.

Another variant is non-contact laser profilometry where reflection of a laser beam from the film surface allows determination of the height profile. This avoids the issue of film damage and also allows film profiles to be obtained throughout the drying process [179].

7.4.2. Laser scanning. A method introduced by Holmes *et al* [98] determined the elevation of the highest point in the film. Casting a film on a substrate with a slight curvature ensures that some point in the film will be the highest. A laser is then scanned vertically until the film is detected. Repeated measurement allows the film height as a function of time to then be followed. The experimental set-up is sketched in figure 27 along with a typical film height profile. The results showed a decline in film height due to evaporation. At some point (point b in figure 27) the drying front passes across the measuring point and a sudden drop in film height is observed. A subsequent drop in film height, of around 3% of the film thickness, is observed at point c. This has now been ascribed to the final portion of the particle consolidation front passing across the observation point. The two-stage packing of particles into a consolidation front is described in section 2.2.1.

7.5. Scattering techniques

The use of scattering techniques to follow the arrangement of particles within a drying film is attractive because of the non-destructive nature of the experiment. The study of drying films will inevitably concern concentrated dispersions and the films will appear opaque. Therefore there are limited applications for light scattering, although there have been a few reports of x-ray and neutron scattering.

7.5.1. Small angle x-ray scattering. Li *et al* [187] report an experiment where SAXS patterns were obtained from a drying film. Because the beam is fixed at one point in space and the various drying fronts pass across the measurement point, different times relate to different points in the drying process. The form factor for the particles is easily obtained from a dilute dispersion and hence the scattering intensity is converted into a structure factor for the particles. The reported structure factors from Li *et al* [187] are shown in figure 28. At early times the particles are in a liquid dispersion with the nearest neighbour peak moving to a larger scattering vector with time, as the average separation decreases. At some time between 84 and 90 s, the particles are captured by the consolidation front and the nearest neighbour peak becomes fixed. In addition the structure factor becomes indicative of a random packing without order.

A similar SAXS result, concerning lack of long range order in dried films, was obtained by Dingenouts and Ballauff [63, 188]. Their system concerned poly(methyl methacrylate) and polystyrene particles, dried well below the glass transition temperature. Although Dingenouts and Ballauff did not follow the dynamics of the drying process their scattering from the dried regions demonstrated a liquid like order, rather than any crystallinity.

7.5.2. Neutron scattering. The use of neutron scattering seems to be fairly limited with respect to drying films. One enormous strength of neutron scattering involves the selective deuteration of different components to enable contrast matching and to only scatter from a particular component in the film. Unlike the in-situ SAXS work of Li *et al* [187] the

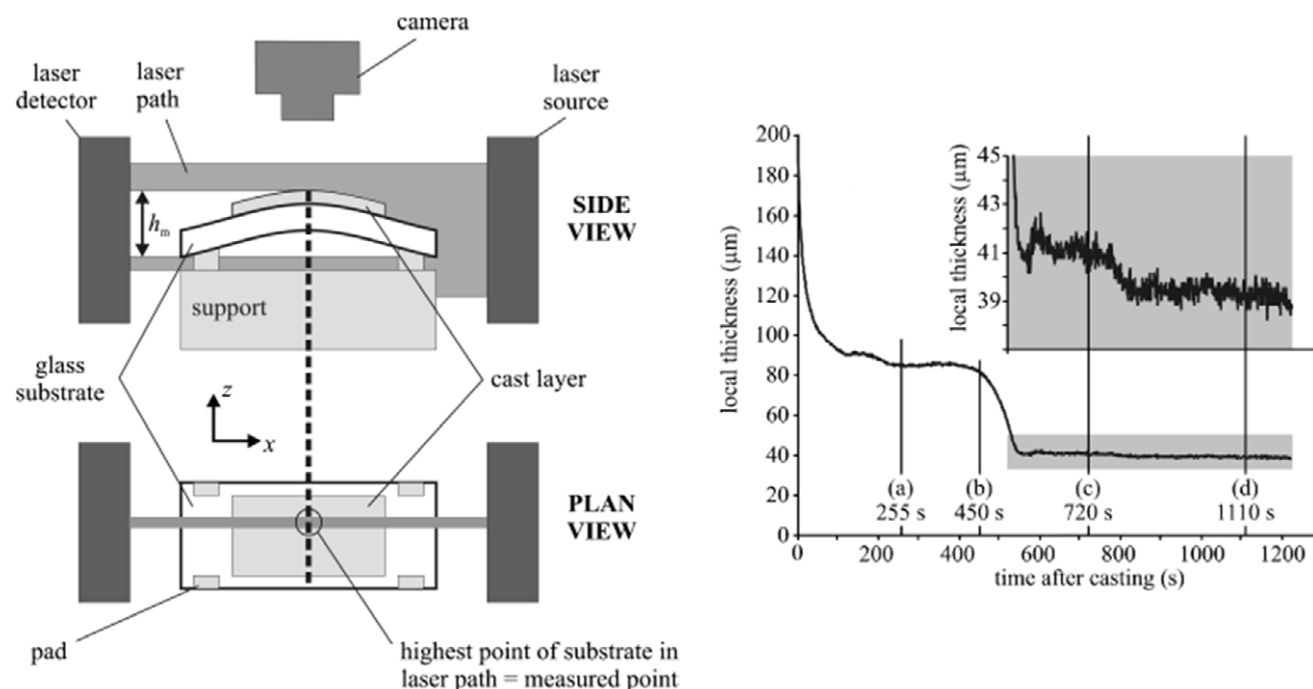


Figure 27. Experimental set-up to follow the height of the thickest part of a film. The substrate is slightly curved and a laser scans vertically to determine the height of the film. A typical result is shown on the right. Up to point (a) the film height reduces because of evaporation and then plateaus up to (b) as the particles start to consolidate. The drying front passes the measuring point and the film height drops considerably before plateauing again at (c). There is a reproducible drop in film height between points (c) and (d) that can be attributed to the irreversible aggregation seen by Goehring *et al* [34]. Images reproduced from [98] with permission from John Wiley and Sons.

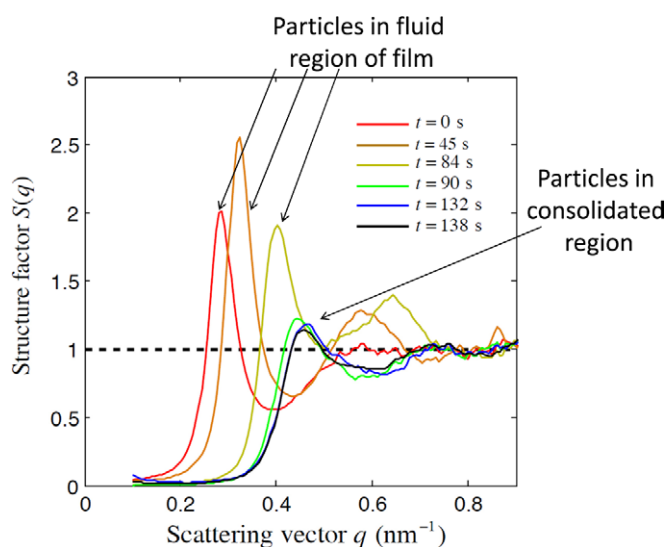


Figure 28. Structures factors determined by SAXS. At early times the scattering is from a colloidal fluid and after 90 s the particles are contained within a disordered solid. Image reprinted with permission from [187]. Copyright (2012) American Chemical Society.

only small angle neutron scattering (SANS) work that could be found related to scattering from pre-dried films. Rieger *et al* [189] examined particle packings in dried films of polymeric particles and showed that larger degrees of crystallinity are observed when the film is dried slowly. Joanicot *et al* [190] examined the loss of scattering intensity from annealed films as latex particles fused together and also demonstrated

the formation of lumps of hydrophilic material within the forming film.

7.6. Measuring composition

As discussed in section 3.1, the arrangement of differing particles at different points within a film will produce multifunctionality and there are many scenarios where this would be advantageous. For example a component with a lower glass transition temperature could be placed closer to a substrate to allow greater adhesion, or an anti-microbial component could be placed near the surface of a film, for use in a sterile environment. There are also numerous examples where a lateral stratification is beneficial. For example a textured coating may require differing properties in the peaks and valleys. As well as beneficial inhomogeneity there are scenarios where accumulation of differing materials can be detrimental. Surfactants within a coating are often found to accumulate in regions of the film, imparting areas with increased hydrophilicity and possibly creating pathways for moisture transport [175, 176]. Therefore measurement of composition at different regions of the film is extremely important.

The microscopy techniques described in section 7.1, such as AFM and electron microscopy, are capable of distinguishing between different particle types. For molecular composition other techniques are required. Confocal Raman spectroscopy, as described in section 7.2.4, has been useful for measuring surfactant concentration. Some other techniques are described in this section. Many of the techniques operate at a surface, which means that obtaining composition profiles through the

film requires a cross-sectional cut. The only technique which can give a depth resolved composition measure, without such sample preparation, is confocal microscopy, although this is then limited by the optical penetration of the measurement beam.

7.6.1. Rutherford back scattering. Rutherford back scattering (RBS) involves measuring the energy of $^4\text{He}^+$ ions, back scattered from a surface. The energy of back scattered ions is dependent on the mass of atoms they scatter from and this provides an elemental map of a surface. RBS is therefore ideal to determine the mass concentration of heavy ions in a matrix of lower molecular mass materials [191]. For soft materials, such as polymers, the helium ions can also penetrate the surface a certain degree, losing energy as they do so. It is therefore possible to obtain composition maps as a function of depth into the film, up to a depth of about half a micrometre [123].

7.6.2. Attenuated total reflection Fourier transform infrared spectroscopy. Attenuated total reflection Fourier transform infrared (ATR-FTIR) spectroscopy operates by placing an ATR crystal in contact with the sample surface. An effervescent wave undergoes multiple reflections along the crystal and passes multiple times through the surface portion of the film. The depth sampled is around $1\ \mu\text{m}$ and the resulting adsorption spectrum is an FTIR spectrum of the top portion of the film, such that surface compositions and concentrations can be determined. The technique has been used extensively by Kunkela and Urban [192] looking at the amounts of surfactant exuded to the surface of films during drying. Gundabala *et al* [62] used ATR-FTIR to examine the surface amounts of surfactant. This was done to critically examine a model linking surface exudation with the drying process and crucially the adsorption isotherm between the particles and surfactant.

7.6.3. X-ray photoelectron spectroscopy. X-ray photoelectron spectroscopy (XPS) operates by irradiating a surface with x-rays and counting the number of electrons emitted at different energies. The energy is a direct measure of the atom at the surface and the number count gives the relative amount. The technique has been extensively used to examine the surface of dried films and to identify different components exuded to the surface. Zhao *et al* [193] followed the exudation of surfactant in films using XPS and showed similar results to an earlier ATR-FTIR study. Zhao *et al* suggest that XPS probes a surface layer as thin as 5 nm and this is far smaller than the micrometre or so probed by ATR-FTIR.

8. Future directions

There are multiple directions for future research within the area of film drying and some specific problems, worthy of study, have been highlighted throughout this article. In this section we list some areas that we believe deserve a concerted effort of investigation, over the next few years.

8.1. Evaporative lithography

The method of evaporative lithography has been initiated by the group of Jennifer Lewis [16–18] and extended by Joe Keddie [20, 21]. As discussed in the introduction, the method involves placing a mask over a drying film. The mask contains holes which only allows evaporation to occur at specified positions in the film. The experimental observation is that the final film profile is elevated in evaporative regions and depressed in non-evaporating regions. The potential of the work is to produce bespoke materials with features on a mm length scale through a single self-assembly processing step. The two independent areas to control within such a film are the film topology and also the composition at different regions within the film. We discuss here how each can be controlled separately: the film topology through fluid mechanics and the film composition through colloid science. As discussed in section 6 the fluid mechanics of thin films is well understood and there are different physical processes that may apply in any specific situation. The different particles may stratify within a film, allowing different properties to be observed in different regions. The simple model outlined in section 3.1 describes balancing diffusion with an imposed velocity to achieve stratification. The work of Atmuri *et al* [57] demonstrates that inter-particle potentials also affect stratification and this suggests that composition within a film is controllable by the particle sizes and interactions.

8.1.1. Fluid mechanics. There are many constituent flows in a thin film subject to spatially variable evaporation. Once particles reach a close-packed state, continued evaporation from this region draws fluid in. The experimental observation is that particles initially consolidate in the region of the film that is evaporating and this is why the final film is higher in this region. Opposing the raised film height is surface tension, which will drive flow against any curvature of the top surface. Two other flows which need to be included are Marangoni and Rayleigh–Bénard convection. Any surfactant exuded to the top surface will locally lower the surface tension and result in Marangoni flows. In addition any heating of the film, for example by an IR lamp, will lead to variations in surface tension and result in flow. The different physical processes that need to be considered are sketched in figure 29 and this is a complicated problem with a multitude of limiting cases and instabilities that require investigation.

Upon solving the flows, the final film profile can be predicted and this allows the mask design to be coupled to the desired film profile. Other parameters that need investigation are the distance between the mask and the film (shown as d on figure 29), as well as the limiting resolution that is achievable from such a configuration.

8.1.2. Stratification. The study of stratification in drying films is in its infancy and deserves further investigation. Trueman *et al* [55, 56] derives the equations governing a diffusive based stratification, although the effect of particle interactions is included in the derivation and Atmuri *et al* [57] demonstrates the effect that these can have. There are a multitude of further areas for research in the general area of

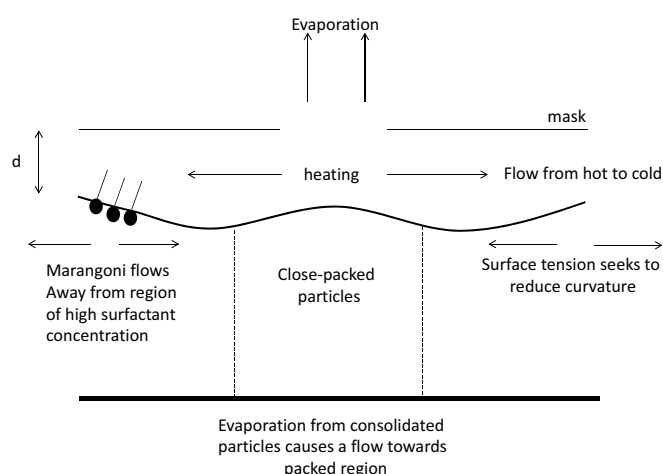


Figure 29. Sketch detailing the flows which need to be considered during evaporative lithography. Consolidated particles at the centre of the film draw fluid in. Any curvature in the film surface is resisted by surface tension. Any non-uniform surfactant concentrations will lead to Marangoni flows and any non-uniform heating will lead to surface tension gradients and flow from hot to cold regions.

stratification. Balancing particle diffusion with a horizontal velocity scale, either the drying front or an induced flow such as a Marangoni flow, will allow a stratification to be observed horizontally within a film. This has been shown experimentally by Harris *et al* [18], using 10 nm polystyrene particles in a mixture of 590 nm silica particles.

The results of Trueman *et al* [55] and Atmuri *et al* [57] display a potential anomaly that is not included in the diffusive theory. The experimental results show a generalized accumulation of small particles at the top surface. The relative amounts of this accumulation can be controlled by altering the Peclet numbers, as suggested by the diffusive theory, however the general accumulation of smaller particles is outside the theory of Trueman *et al* [56]. One possibility is that the surface properties of the small particles causes an accumulation at the top surface and this is shown theoretically by Atmuri [57]. Another possibility is that the flow of small particles through the larger ones, as described by Luo *et al* [59] is occurring, although it is noted that the particle size difference is not large enough for a free passage of smaller particles. The possibility remains that a different flow is occurring and this is carrying the smaller particles to the top surface. The origin of such a flow could be Marangoni or temperature, or indeed something else all together. Further study is warranted.

8.2. Control over film topology

The overall aim of many drying processes is to obtain a desired film profile. Indeed for many situations it is desired to have as flat a final film profile as possible. In any given system, most physical parameters such as viscosity and surface tension are fixed and this results in only very limited control variables. The evaporative lithography process provides a way that control over the spatial variation in evaporation can lead to a patterned final film, although this method will not work to achieve a flat film. Without using a mask, one possible control parameter

is the drying rate. For a given situation, it may be possible to locally cycle the humidity to turn evaporation on and off. Indeed it may even be possible to precipitate solvent back from a humid atmosphere, by increasing the relative humidity above 100% [194, 195]. The result of such a strategy would be to change the magnitude, and possibly even the sign, of the evaporative term \dot{E} in equation (7). Finding an optimal evaporation profile through time, to give the desired final film profile becomes an optimal control problem on equations (7) and (8). This may seem a counterintuitive way to proceed, because turning off evaporation can only prolong the drying process. However, providing more time for surface tension to flatten films and also allowing any surfactant concentration gradients to dissipate allowed Kajiya and Doi to achieve flatter final films [194, 195]. The solution of the control problem will allow an optimal solution to be obtained for the desired final profile and such a method seems ideally suited to obtain flat films. The next step in such a research area will be to simulate equations (7) and (8) and to experimentally examine such numerical predictions.

8.3. Varying substrate properties

Throughout this article the implicit assumption has been made that the substrate is impermeable. This is not necessarily the case and a study of permeable substrates, with the resulting impact on final film topologies is certainly warranted. In addition Smith and Sharp [75] demonstrated the effect of substrate compliance on film cracking, with weaker substrates resulting in larger crack spacings. Combining the two effects and examining the effect of substrate permeability on the cracking in thin films is, to the authors best knowledge, an unexplored area.

9. Conclusions

Work in the area of drying colloidal films has expanded rapidly in the past few years. There are numerous potential applications, especially in the area of self-assembled materials generation, and this has been used in evaporative lithography.

The control over film profile and composition requires an understanding of the various transitions that can occur as a colloidal film dries. This article reports the observations of drying experiments where numerous fronts are seen to traverse laterally across films. These are ascribed to particle packing, cracking, dewetting and potentially optical clarity fronts. The physics of the formation of such fronts has been explained and the crucial physical parameter is shown to be the capillary pressure, which is generated in the solidified region of the film.

Non-uniform particle arrangement is a common occurrence, and this is explored within a diffusive framework that balances particle diffusion against an imposed velocity scale. When particle diffusion is strong the volume fraction is predicted to be uniformly distributed and when convection dominates particle non-uniformities appear. This can be used to stratify films which contain two or more particle types. The

result is films with spatially variable compositions and hence multifunctional materials.

The evaporation from films has been explored. It has been shown that large films in non-stagnant air will display a spatially uniform evaporation rate. For small drops of fluid an enhanced evaporation rate at the drop edge is predicted and this increases with smaller contact angles.

It is common to use lubrication theory for describing the flows in evaporating films, and this leads to fourth order partial differential equations to describe the evolution of film height and particle volume fraction. The main flow in an evaporating colloidal film occurs towards consolidated regions of particles. This is because of continued evaporation from packed particles. In addition flows that commonly occur are Marangoni and Rayleigh–Bénard convection which arise from surfactant concentration and temperature non-uniformities.

Finally this article lists a number of experimental techniques that have been used to examine drying films. The parameters of interest are film height, film stress, particle arrangement, and the location of water and other small additives, such as surfactant.

The area of colloidal film drying has been active for a large number of years. It is of interest to the fluid mechanics community, with a range of theoretical problems to solve. In addition experimentalists have developed a range of techniques to probe various aspects. Colloid scientists are interested with the possibility of templating films through control over the inter-particle potential of the constituent particles. It is hoped that this article has demonstrated that colloidal film drying is a rich multi-disciplinary area that will continue to grow for a number of years yet.

Acknowledgments

The author is extremely grateful to the array of students and post-docs who have worked in the area of film drying with him. These include undergraduate projects with David Gibney, Tom Collins, Sylvain Caron, Michael Johnson, Nick Petty, Polly Keen, Andrew Cheetwood, Rebecca Conroy and Asad Akhter, PhD projects with Wei Peng Lee, Venkata Gundabala, Richard Trueman and Adam Eales and post-doc projects with Milan Patel, Grace Yow and Lucas Goehring. The author has been extremely fortunate to have had the opportunity to work with many collaborators in both academia and industry. The industrialists have included Malcolm Faers at Bayer Crop Sciences, Martin Murray, Simon Emmett and Elsa Lago-Domingues at AkzoNobel, Nick Dartnell at Cambridge Display Technology and Andrew Howe at Kodak and now Schlumberger. In academia the author was introduced to the issue of colloids and thin films by Bill Russel and has been extremely fortunate to work closely with Bill Clegg at Cambridge and Diethelm Johannsmann at Clausthal. In addition Joe Keddie at the University of Surrey has been a constant source of ideas, encouragement and collaboration over the past 12 years.

In addition the author is very grateful for the funding that has supported this research. This has been from a number of

sources including EPSRC, EU Framework 6 project Napoleon, AkzoNobel and CDT.

Finally the author wishes to thank Athene Donald for the opportunity to write this review.

References

- [1] Russel W B, Saville D A and Schowalter W R 1991 *Colloidal Dispersions* (Cambridge: Cambridge University Press)
- [2] Hunter R J 1985 *Colloid Science* (Oxford: Oxford University Press)
- [3] Deegan R D, Bakajin O, Dupont T F, Huber G, Nagel S R and Witten T A 1997 Capillary flow as the cause of ring stains from dried liquid drops *Nature* **389** 827–9
- [4] Sheetz D P 1965 Formation of films by drying of latex *J. Appl. Polym. Sci.* **9** 3759–73
- [5] Goehring L, Conroy R, Akhter A, Clegg W J and Routh A F 2010 Evolving mud crack patterns *Soft Matter* **6** 3562–7
- [6] Wu Y, Eliyahu J, Liu P and Hu N-X 2012 Solvent based inks comprising silver nanoparticles *US Patent Application* US 2012/0232206 A1
- [7] van Dam D B and Kuertan J G M 2008 Modeling the drying of ink-jet-printed structures and experimental verification *Langmuir* **24** 582–9
- [8] Gaskin R E (ed) 2007 Annulus spray deposit structures and enhanced ai-adjuvant association with adjuvanted flowables *Proc. 8th Int. Symp. on Adjuvants for Agrochemicals (ASAA2007)* (Columbus, OH, USA) (The Netherlands: International Society for Agrochemical Adjuvants)
- [9] Faers M A and Pontzen R 2008 Factors influencing the association between active ingredient and adjuvant in the leaf deposit of adjuvant containing suspoemulsion formulations *Pest Manag. Sci.* **64** 820–33
- [10] Willmer D, Baldwin K A, Kwartnik C and Fairhurst D J 2010 Growth of solid conical structures during multistage drying of sessile poly(ethylene oxide) droplets *Phys. Chem. Chem. Phys.* **12** 3998–4004
- [11] Baldwin K A, Granjard M, Willmer D I, Sefiane K and Fairhurst D J 2011 Drying and deposition of poly(ethylene oxide) droplets determined by peclet number *Soft Matter* **7** 7819–26
- [12] Baldwin K A, Roest S, Fairhurst D J, Sefiane K and Shanahan M E R 2012 Monolith formation and ring-stain suppression in low-pressure evaporation of poly(ethylene oxide) droplets *J. Fluid Mech.* **695** 321–9
- [13] Kajiyama T, Nishitani E, Yamaue T and Doi M 2006 Piling-to-buckling transition in the drying process of polymer solution drop on substrate having a large contact angle *Phys. Rev. E* **73** 011601
- [14] Head D A 2006 Modeling the elastic deformation of polymer crusts formed by sessile droplet evaporation *Phys. Rev. E* **74** 021601
- [15] Han W and Lin Z 2012 Learning from ‘coffee rings’: ordered structures enabled by controlled evaporative self-assembly *Angew. Chem. Int. Ed.* **51** 1534–46
- [16] Harris D J, Hu H, Conrad J C and Lewis J A 2007 Patterning colloidal films via evaporative lithography *Phys. Rev. Lett.* **98** 148301
- [17] Harris D J and Lewis J A 2008 Marangoni effects on evaporative lithographic patterning of colloidal films *Langmuir* **24** 3681–5
- [18] Harris D J, Conrad J C and Lewis J A 2009 Evaporative lithographic patterning of binary colloidal films *Phil. Trans. R. Soc. A* **367** 5157–65
- [19] Parneix C, Vandoolaeghe P, Nikolayev V S, Quere D, Li J and Cabane B 2010 Dips and rims in dried colloidal films *Phys. Rev. Lett.* **105** 266103

- [20] Georgiadis A, Routh A F, Murray M W and Keddie J L 2011 Bespoke periodic topography in hard polymer films by infrared radiation-assisted evaporative lithography *Soft Matter* **7** 11098–102
- [21] Georgiadis A, Bryant P A, Murray M W, Beharrell P and Keddie J L 2011 Resolving the film formation dilemma with infrared radiation assisted sintering *Langmuir* **27** 2176–80
- [22] Keddie J L and Georgiadis A 2010 A method of making a hard latex and and hard latex *World Patent Application* WO 2010/097592
- [23] Georgiadis A, Muhamad F N and Keddie J L 2013 Aesthetically-textured hard latex coatings by fast IR-assisted evaporative lithography *Prog. Org. Coat.* accepted
- [24] Utgenannt A, Keddie J L, Muskens O L and Kanaras A G 2013 Directed organisation of gold nanoparticles in polymer coatings through infrared-assisted evaporative lithography *Chem. Commun.* Advance article DOI:10.1039/C2CC37844B
- [25] Arshad T A and Bonnezaze R T 2013 Templated evaporative lithography for high throughput fabrication of nanopatterned films *Nanoscale* **5** 624–33
- [26] Keddie J L and Routh A F 2010 *Fundamentals of Latex Film Formation: Processes and Properties* (Springer Laboratory) (Berlin: Springer)
- [27] Keddie J L 1997 Film formation of latex *Mater. Sci. Eng. R* **21** 101–70
- [28] Yunker P J, Still T, Lohr M A and Yodh A G 2011 Suppression of the coffee-ring effect by shape dependent capillary interactions *Nature* **476** 308–11
- [29] Eral H B, Mampallil Augustine D, Duits M H G and Mugele F 2011 Suppressing the coffee stain effect: how to control colloidal self-assembly in evaporating drops using electrowetting *Soft Matter* **7** 4954–8
- [30] Shmuylovich L, Shen A Q and Stone H A 2002 Surface morphology of drying latex films: multiple ring formation *Langmuir* **18** 3441–5
- [31] White L R 1982 Capillary rise in powders *J. Colloid Interface Sci.* **90** 536–8
- [32] Routh A F and Russel W B 1999 A process model for latex film formation: limiting regimes for individual driving forces *Langmuir* **15** 7762–73
- [33] Salamanca J M, Ciampi E, Faux D A, Glover P M, McDonald P J, Routh A F, Peters A C I A, Satguru R and Keddie J L 2001 Lateral drying in thick films of waterborne polymer colloids *Langmuir* **17** 3202–8
- [34] Goehring L, Clegg W J and Routh A F 2010 Solidification and ordering during drying of a colloidal dispersion *Langmuir* **26** 9269–75
- [35] Routh A F, Russel W B, Tang J and El-Aasser M S 2001 A process model for latex film formation: optical drying fronts *J. Coat. Technol.* **73** 41–8
- [36] Hodges C S, Ding Y and Biggs S 2010 The influence of nanoparticle shape on the drying of colloidal dispersions *J. Colloid Interface Sci.* **352** 99–106
- [37] Haw M D, Gillie M and Poon W C K 2001 Effects of phase behaviour on the drying of colloidal suspensions *Langmuir* **18** 1626–33
- [38] Ma Y, Davis H T and Scriven L E 2005 Microstructure development in drying latex coatings *Prog. Org. Coat.* **52** 46–62
- [39] Petersen C, Heldmann C and Johannsmann D 1999 Internal stresses during film formation of polymer latices *Langmuir* **15** 7745–51
- [40] Tirumkudulu M S and Russel W B 2004 Role of capillary stresses in film formation *Langmuir* **20** 2947–61
- [41] Yow H N, Beristain I, Goikeotxea M, Barandiaran M J and Routh A F 2010 Evolving stresses in latex films as a function of temperature *Langmuir* **26** 6335–42
- [42] Yow H N, Goikeotxea M, Goehring L and Routh A F 2010 Effect of film thickness and particle size on cracking stresses in drying latex films *J. Colloid Interface Sci.* **352** 542–8
- [43] Vanderhoff J W, Bradford E B and Carrington W K 1973 The transport of water through latex films *J. Polym. Sci.* **41** 155–74
- [44] Croll S G 1986 Drying of latex paint *J. Coat. Technol.* **58** 41–9
- [45] Croll S G 1987 Heat and mass transfer in latex paints during drying *J. Coat. Technol.* **59** 81–92
- [46] Reyes Y and Duda Y 2005 Modeling of drying in films of colloidal particles *Langmuir* **21** 7057–60
- [47] Routh A F and Zimmerman W B 2004 Distribution of particles during solvent evaporation from films *Chem. Eng. Sci.* **59** 2961–8
- [48] Ekanayake P, McDonald P J and Keddie J L 2009 An experimental test of the scaling prediction for the spatial distribution of water during the drying of colloidal films *Euro. Phys. J. Spec. Top.* **166** 21–7
- [49] Narita T, Hebraud P and Lequeux F 2005 Effects of the rate of evaporation and film thickness on the nonuniform drying of film-forming concentrated colloidal suspensions *Euro. Phys. J. E* **17** 69–76
- [50] König A M, Weerakkody T G, Keddie J L and Johannsmann D 2008 Heterogeneous drying of colloidal polymer films: dependence on added salt *Langmuir* **24** 7580–9
- [51] Sarkar A and Tirumkudulu M S 2009 Consolidation of charged colloids during drying *Langmuir* **25** 4945–53
- [52] Buss F, Roberts C C, Crawford K S, Peters K and Francis L F 2011 Effect of soluble polymer binder on particle distribution in a drying particulate coating *J. Colloid Interface Sci.* **359** 112–20
- [53] Shimmin R G, DiMauro A J and Braun P V 2006 Slow vertical deposition of colloidal crystals: a langmuir-blodgett process? *Langmuir* **22** 6507–13
- [54] Cardinal C M, Jung Y D, Ahn K H and Francis L F 2010 Drying regime maps for particulate coatings *AIChE J.* **56** 2769–80
- [55] Trueman R E, Lago Domingues E, Emmett S N, Murray M and Routh A F 2012 Auto-stratification in drying colloidal dispersions: a diffusive model *J. Colloid Interface Sci.* **377** 207–12
- [56] Trueman R E, Lago Domingues E, Emmett S N, Murray M, Keddie J L and Routh A F 2012 Auto-stratification in drying colloidal dispersions: experimental investigations *Langmuir* **18** 3420–8
- [57] Atmuri A, Bhatia S R and Routh A F 2012 Auto-stratification in drying colloidal dispersions: effect of particle interactions *Langmuir* **28** 2652–8
- [58] Nikiforow I, Adams J, König A M, Langhoff A, Phol K, Turshatov A and Johannsmann D 2010 Self-stratification during film formation from latex blends driven by differences in collective diffusivity *Langmuir* **26** 13162–7
- [59] Luo H, Cardinal C M, Scriven L E and Francis L F 2008 Ceramic nanoparticle/monodisperse latex coatings *Langmuir* **24** 5552–61
- [60] Lei C H, Ouzineb K, Dupont O and Keddie J L 2007 Probing particle structure in waterborne pressure-sensitive adhesives with atomic force microscopy *J. Colloid Interface Sci.* **307** 56–63
- [61] Gundabala V R, Lei C H, Ouzineb K, Dupont O, Keddie J L and Routh A F 2008 Lateral surface nonuniformities in drying latex films *AIChE J.* **54** 3092–105

- [62] Gundabala V R, Zimmerman W B and Routh A F 2004 A model for surfactant distribution in latex coatings *Langmuir* **20** 8721–7
- [63] Dingenouts N and Ballauff M 1999 First stage of film formation by latexes investigated by small angle x-ray scattering *Langmuir* **15** 3283–8
- [64] Mallegol J, Bennett G, McDonald P J and Keddie J L 2006 Skin development during the film formation of waterborne acrylic pressure-sensitive adhesives containing tackifying resin *J. Adhes.* **82** 217–38
- [65] Ciampi E and McDonald P J 2003 Skin formation and water distribution in semicrystalline polymer layers cast from solution: a magnetic resonance imaging study *Macromolecules* **36** 8398–405
- [66] Wallin M, Glover P M, Hellgren A C, Keddie J L and McDonald P J 2000 Depth profiles of polymer mobility during the film formation of a latex dispersion undergoing photoinitiated cross-linking *Macromolecules* **33** 8443–52
- [67] Juillerat F, Bowen P and Hoffman H 2006 Formation and drying of colloidal crystals using nanosized silica particles *Langmuir* **22** 2249–57
- [68] Zhou Z, Li Q and Zhao X S 2006 Evolution of interparticle capillary forces during drying of colloidal crystals *Langmuir* **22** 3692–7
- [69] Bucklow S 1997 The description of craquelure patterns *Stud. Conservation* **42** 129–40
- [70] Bucklow S 1999 Description and classification of craquelure *Stud. Conservation* **44** 233–44
- [71] Ball P 2004 Material witness: watching paint dry *Nature Mater.* **3** 851
- [72] Walker J 1986 The amateur scientist: cracks in a surface look intricately random but actually develop rather systematically *Sci. Am.* **255** 204–11
- [73] Chiu R C, Garino T J and Cima M J 1993 Drying of granular ceramic films: I. Effect of processing variables on cracking behavior *J. Am. Ceram. Soc.* **76** 2257–64
- [74] Chiu R C and Cima M J 1993 Drying of granular ceramic films: II. Drying stress and saturation uniformity *J. Am. Ceram. Soc.* **76** 2769–77
- [75] Smith M I and Sharp J S 2011 Effects of substrate constraint on crack pattern formation in thin films of colloidal polystyrene particles *Langmuir* **27** 8009–17
- [76] Tarafdar S and Sinha S 2008 Crack formation in dryin glaponite *Indust. Eng. Chem. Res.* **47** 6459–64
- [77] Neda Z, Leung K t, Jozsa L and Ravasz M 2002 Spiral cracks in drying precipitates *Phys. Rev. Lett.* **88** 5502
- [78] Lazarus V and Pauchard L 2011 From craquelures to spiral crack patterns: influence of layer thickness on the crack patterns induced by desiccation *Soft Matter* **7** 2552–9
- [79] Goehring L, Clegg W J and Routh A F 2011 Wavy cracks in drying colloidal films *Soft Matter* **7** 7984–7
- [80] Jing G and Ma J 2012 Formation of circular crack pattern in deposition self-assembled by drying nanoparticle suspension. *J. Phys. Chem. B* **116** 6225–31
- [81] Pauchard L, Adda-Bedia M, Allain C and Couder Y 2003 Morphologies resulting from the directional propagation of fractures *Phys. Rev. E* **67** 7103
- [82] Hopfield J J 1946 Spiral cracks in glass tubes *Nature* **158** 582–3
- [83] Yuse A and Sano M 1993 Transition between crack patterns in quenched glass plates *Nature* **362** 329–31
- [84] Sasa S, Sekimoto K and Nakanishi H 1994 Oscillatory instability of crack propagations in quasistatic fracture *Phys. Rev. E* **50** 1733–6
- [85] Adda-Bedia M and Pomeau Y 1995 Crack instabilities of a heated glass strip *Phys. Rev. E* **52** 4105–13
- [86] Marder M 1994 Instability of a crack in a heated strip *Phys. Rev. E* **49** 51–4
- [87] Boeck T, Bahr H A, Lampenscherf S and Bahr U 1999 Self-driven propagation of crack arrays: a stationary two-dimensional model *Phys. Rev. E* **59** 1408–16
- [88] Yuse A and Sano M 1997 Instabilities of quasi-static crack patterns in quenched glass plates *Physica D* **108** 365–78
- [89] Yang B and Ravi-Chandar K 2001 Crack path instabilities in a quenched glass plate *J. Mech. Phys. Solids* **49** 91–130
- [90] Groisman A and Kaplan E 1994 An experimental study of cracking induced by desiccation *Europhys. Lett.* **25** 415–20
- [91] Bohn S, Pauchard L and Couder Y 2005 Hierarchical crack pattern as formed by successive domain divisions: I. Temporal and geometrical hierarchy *Phys. Rev. E* **71** 046214
- [92] Gauthier G, Lazarus V and Pauchard L 2010 Shrinkage star-shaped cracks: explaining the transition from 90 degrees to 120 degrees *Eur. Phys. Lett.* **89** 6002
- [93] Shorlin K A, de Bruyn J R, Graham M and Morris S W 2000 Development and geometry of isotropic and directional shrinkage-crack patterns *Phys. Rev. E* **61** 6950–7
- [94] Gabrielli A, Cafiero R and Caldarelli G 1999 Statistical properties of fractures in damaged materials *Europhys. Lett.* **45** 13–9
- [95] Korvin G 1989 Fractured but not fractal: fragmentation of the gulf of Suez basement *Pure Appl. Geophys.* **131** 289–305
- [96] Bohn S, Platkiewicz J, Andreotti B, Adda-Bedia M and Couder Y 2005 Hierarchical crack pattern as formed by successive domain divisions: II. From disordered to deterministic behaviour *Phys. Rev. E* **71** 046215
- [97] Tirumkudulu M S and Russel W B 2006 Cracking in drying latex films *Langmuir* **21** 4938–48
- [98] Holmes D M, Kumar R V and Clegg W J 2006 Cracking during lateral drying of alumina suspensions *J. Am. Ceram. Soc.* **89** 1908–13
- [99] Dufresne E R, Corwin E I, Greenblatt N A, Ashmore J, Wang D Y, Dinsmore A D, Cheng J X, Xie X S, Hutchinson J W and Weitz D A 2003 Flow and fracture in drying nanoparticle suspensions *Phys. Rev. Lett.* **91** 4501
- [100] Dufresne E R, Stark D J, Greenblatt N A, Cheng J X, Hutchinson J W, Mahadevan L and Weitz D A 2006 Dynamics of fracture in drying suspensions *Langmuir* **22** 7144–7
- [101] Lei H, Payne J A, McCormick A V, Francis L F, Gerberich W W and Scriven L E 2001 Stress development in drying coatings *J. Appl. Poly. Sci.* **81** 1000–13
- [102] Lei H, Francis L F, Gerberich W W and Scriven L E 2002 Stress development in drying coatings after solidification *AIChE J.* **48** 437–51
- [103] Cotterell B and Rice J R 1980 Slightly curved or kinked cracks *Int. J. Fract.* **16** 155–169
- [104] Beuth J L 1992 Cracking of thin bonded films in residual tension. *Int. J. Solids Struct.* **29** 1657–75
- [105] Goehring L, Clegg W J and Routh A F 2013 Plasticity and fracture in drying colloidal films *Phys. Rev. Lett.* **110** 024301
- [106] Bordia R K and Jagota A 1993 Crack growth and damage in constrained sintering films *J. Am. Ceram. Soc.* **76** 2475–85
- [107] Jagota A and Hui C Y 1990 Mechanics of sintering thin films: I. Formulation and analytical results *Mech. Mater.* **9** 107–19
- [108] Jagota A and Hui C Y 1991 Mechanics of sintering thin films: II. Cracking due to self-stress *Mech. Mater.* **11** 221–34
- [109] Ye T, Suo Z and Evans A G 1992 Thin film cracking and the roles of substrate and interface *Int. J. Solids Struct.* **29** 2639–48

- [110] Nahta R and Moran B 1995 Crack spacing in brittle films on dissimilar planar and axisymmetric elastic substrates *Eng. Fract. Mech.* **52** 513–24
- [111] Beuth J L and Klingbeil N W 1996 Cracking in thin films bonded to elastic-plastic substrates *J. Mech. Phys. Solids* **44** 1411–28
- [112] Schulze G W and Erdogan F 1998 Periodic cracking of elastic coatings *Int. J. Solids Struct.* **35** 3615–34
- [113] Parker A P 1999 Stability of arrays of multiple edge cracks *Eng. Fract. Mech.* **62** 577–91
- [114] Xia Z C and Hutchinson J W 2000 Crack patterns in thin films *J. Mech. Phys. Solids* **48** 1107–31
- [115] Bai T, Pollard D D and Gao H 2000 Explanation for fracture spacing in layered materials *Nature* **403** 753–6
- [116] Adda-Bedia M and Ben Amar M 2001 Fracture spacing in layered materials *Phys. Rev. Lett.* **86** 9007
- [117] Hull D and Caddock B D 1999 Simulation of prismatic cracking of cooling basalt lava by the drying of sol-gels *J. Mater. Sci.* **34** 5707–20
- [118] Lee W P and Routh A F 2004 Why do drying films crack? *Langmuir* **20** 9885–8
- [119] Jagla E A 2002 Stable propagation of an ordered array of cracks during directional drying *Phys. Rev. E* **65** 046147
- [120] Allain C and Limat L 1995 Regular patterns of cracks formed by directional drying of a colloidal suspension *Phys. Rev. Lett.* **74** 2981–4
- [121] Komatsu T S and Sasa S I 1997 Pattern selection of cracks in directionally drying fracture *Japan. J. Appl. Phys.* **36** 391–5
- [122] Gauthier G, Lazarus V and Pauchard L 2007 Alternating crack propagation during directional drying *Langmuir* **23** 4715–8
- [123] Lee W P and Routh A F 2006 Temperature dependence of crack spacing in drying latex films *Indust. Eng. Chem. Res.* **45** 6996–7001
- [124] Singh K B and Tirumkudulu M S 2007 Cracking in drying colloidal films *Phys. Rev. Lett.* **98** 218302
- [125] Singh K B, Bhosale L R and Tirumkudulu M S 2009 Cracking in drying colloidal films of flocculated dispersions *Langmuir* **25** 4284–7
- [126] Pauchard L and Parris C and Allain F 1999 Influence of salt content on crack patterns formed through colloidal suspension desiccation *Phys. Rev. E* **59** 3737–40
- [127] Kanai T and Sawada T 2009 New route to produce dry colloidal crystals without cracks *Langmuir* **25** 12215–3317
- [128] Tzitzinou A, Keddie J L, Geurts J M, Peters A C I A and Satguru R 2000 Film formation of latex blends with bimodal particle size distributions: consideration of particle deformability and continuity of the dispersed phase *Macromolecules* **33** 2695–708
- [129] Singh K B, Deoghare G and Tirumkudulu M S 2009 Cracking in soft-hard latex blends: theory and experiments *Langmuir* **25** 751–60
- [130] Winnik M A and Feng J 1996 Latex blends: an approach to zero VOC coatings *J. Coat. Technol.* **68** 39–50
- [131] Qiao J, Adams J and Johannsmann D 2012 Addition of halloysite nanotubes prevents cracking in drying latex films *Langmuir* **28** 8674–80
- [132] Bellet D and Canham L 1998 Controlled drying; the key to better quality porous semiconductors *Adv. Mater.* **10** 487–90
- [133] Picknett R G and Bexon R 1977 The evaporation of sessile or pendant drops in still air *J. Colloid Interface Sci.* **61** 336–50
- [134] Erbil H Y, McHale G and Newton M I 2002 Drop evaporation on solid surfaces: constant contact angle mode *Langmuir* **18** 2636–41
- [135] Popov Y O 2005 Evaporative deposition patterns: spatial dimension of the deposit *Phys. Rev. E* **71** 036313
- [136] Deegan R D 2000 Pattern formation in drying drops *Phys. Rev. E* **61** 475–85
- [137] Deegan R D, Bakajin O, Dupont T F, Huber G, Nagel S R and Witten T A 2000 Contact line deposits in an evaporating drop *Phys. Rev. E* **62** 756–65
- [138] Hu H and Larson R G 2002 Evaporation of a sessile droplet on a substrate *J. Phys. Chem. B* **106** 1334–44
- [139] Routh A F and Russel W B 1998 Horizontal drying fronts during solvent evaporation from latex films *AIChE J.* **44** 2088–98
- [140] Fischer B J 2002 Particle convection in an evaporating droplet *Langmuir* **18** 60–7
- [141] de Gans B J and Schubert U S 2004 Inkjet printing of well-defined polymer dots and arrays *Langmuir* **20** 7789–93
- [142] O'Brien F E M 1948 The control of humidity by saturated salt solutions *J. Sci. Instrum. Phys. Industry* **25** 73–6
- [143] Rockland L B 1960 Saturated salt solutions for static control of relative humidity between 5 °C and 40 °C *Anal. Chem.* **32** 1375–6
- [144] Haines W B 1920 Studies in the physical properties of soil: V. The hysteresis effect in capillary properties and the modes of moisture distribution associated therewith *J. Agric. Sci.* **20** 97–116
- [145] Haas A and Revil A 2009 Electrical burst signature of pore-scale displacements *Water Resources Res.* **45** 10202
- [146] Herbert E, Balibar S and Caupin F 2006 Cavitation pressure in water *Phys. Rev. E* **74** 1603
- [147] Kohonen M M 2006 Engineered wettability in tree capillaries *Langmuir* **22** 3148–53
- [148] Oron A, Davis S H and Bankoff S G 1997 Long-scale evolution of thin liquid films *Rev. Mod. Phys.* **69** 931–80
- [149] Craster R V and Matar O K 2009 Dynamics and stability of thin liquid films *Rev. Mod. Phys.* **81** 1131–98
- [150] Leal L G 1992 *Laminar Flow and Convective Transport Processes: scaling Principles and Asymptotic Analysis* (Butterworth-Heinemann Series in Chemical Engineering) (Boston, MA: Butterworth-Heinemann)
- [151] Zimmerman W B, Rees J M and Hewakandamby B N 2007 Numerical analysis of solutocapillary marangoni-induced interfacial waves *Adv. Colloid Interface Sci.* **134–135** 346–59
- [152] Gundabala V R and Routh A F 2006 Thinning of drying latex films under the action of surfactant *J. Colloid Interface Sci.* **303** 306–14
- [153] Yiantsios S G and Higgins B G 2006 Marangoni flows during drying of colloidal films *Phys. Fluids* **18** 082103
- [154] Troian S M, Wu X L and Safran S A 1989 Fingering instability in thin wetting films *Phys. Rev. Lett.* **62** 1496–1500
- [155] Yiantsios S G and Higgins B G 2010 A mechanism of marangoni instability in evaporating thin liquid films due to soluble surfactant *Phys. Fluids* **22** 022102
- [156] Block M J 1956 Surface tension as the cause of Benard cells and surface deformation in a liquid film *Nature* **178** 650–1
- [157] Vanhook S J, Schatz M F, Swift J B, McCormick M F and Swinney H L 1997 Long-wavelength surface tension driven benard convection: experiment and theory *J. Fluid Mech.* **345** 45–78
- [158] Pearson J R A 1958 On convection cells induced by surface tension *J. Fluid Mech.* **4** 489–500
- [159] Okuzono T, Kobayashi M and Doi M 2009 Final shape of a drying thin film *Phys. Rev. E* **80** 021603
- [160] Kobayashi M, Makino M, Okuzono T and Doi M 2010 Interference effect in the drying of polymer droplets on substrate *J. Phys. Soc. Japan* **79** 4802

- [161] Wang J and Evans J R G 2006 Segregation in multicomponent ceramic colloids during drying of droplets *Phys. Rev. E* **73** 021501
- [162] Weonm B M and Je J H 2010 Capillary force repels coffee-ring effect *Phys. Rev. E* **82** 015305
- [163] Bastacky J, Wodley C, LaBrie R and Backhus C 1987 A bibliography of low-temperature scanning electron microscopy (LTSEM, cryo-SEM) and scanning electron microscopy of frozen hydrated biological systems *Scanning* **9** 219–25
- [164] Luo H, Scriven L E and Francis L F 2007 Cryo-SEM studies of latex/ceramic nanoparticle coating microstructure development *J. Colloid Interface Sci.* **316** 500–9
- [165] Danilatos G D 1993 Introduction to the ESEM instrument *Microsc. Res. Techn.* **25** 354–61
- [166] Keddie J L, Meredith P, Jones R A L and Donald A M 1995 Kinetics of film formation in acrylic latices studied with multiple-angle-of-incidence ellipsometry and environmental SEM *Macromolecules* **28** 1673–2682
- [167] Keddie J L, Meredith P, Jones R A L and Donald A M 1996 Film formation of acrylic latices with varying concentrations of non-film-forming latex particles *Langmuir* **12** 3793–801
- [168] Dragnevski K I, Routh A F, Murray M W and Donald A M 2010 Cracking in drying latex films: an ESEM experiment *Langmuir* **26** 7747–51
- [169] Tzitzinou A, Jenneson P M, Clough A S, Keddie J L, Lu J R, Zhdan P, Treacher K E and Satguru R 1999 Surfactant concentration and morphology at the surfaces of acrylic latex films *Prog. Org. Coat.* **35** 89–99
- [170] Mallegol J, Dupont O and Keddie J 2003 Morphology and elasticity of waterborne acrylic pressure-sensitive adhesives investigated with atomic force microscopy *J. Adhes. Sci.* **17** 243–59
- [171] Mantle M D and Sederman A J 2003 Dynamic MRI in chemical process and reaction engineering *Prog. Nucl. Magn. Reson. Spectrosc.* **43** 3–60
- [172] Glover P M, Aptaker P S, Bowler J R, Ciampi E and McDonald P J 1999 A novel high-gradient permanent magnet for the profiling of planar films and coatings *J. Magn. Reson.* **139** 90–7
- [173] Ludwig I, Schabel W, Kind M, Castaing J C and Ferlin P 2007 Drying and film formation of industrial waterborne latices *AIChE J.* **53** 549–60
- [174] Ludwig I, Schabel W, Ferlin P, Castaing J C and Kind M 2009 Drying, film formation and open time of aqueous polymer dispersions *Eur. Phys. J. Spec. Top.* **166** 39–43
- [175] Arnold C, Thalmann F, Marques C, Marie Y and Holl P 2010 Surfactant distribution in waterborne acrylic films: I. Bulk investigation *J. Phys. Chem. B* **114** 9135–47
- [176] Arnold C, Klein G, Maaloum M, Ernstsson M, Larsson A, Marie Y and Holl P 2011 Surfactant distribution in waterborne acrylic films: II. Surface investigation *Colloids Surf. A* **374** 58–68
- [177] Francis L F, McCormick A V, Vaessen D M and Payne J A 2002 Development and measurement of stress in polymer coatings *J. Mater. Sci.* **37** 4717–31
- [178] Wedin P, Lewis J A and Bergstrom L 2005 Soluble organic additive effects on stress development during drying of calcium carbonate suspensions *J. Colloid Interface Sci.* **290** 134–44
- [179] Martinez C J and Lewis J A 2002 Shape evolution and stress development during latex-silica film formation *Langmuir* **18** 4689–98
- [180] von der Ehe K and Johannsmann D 2007 Maps of the stress distribution in drying latex films *Rev. Sci. Instrum.* **78** 113904
- [181] König A M and Johannsmann D 2010 Stress fluctuations in drying polymer dispersions *Langmuir* **26** 9437–41
- [182] König A M, Bourgeat-Lami E, Mellon V, von der Ehe K, Routh A F and Johannsmann D 2010 Dilational lateral stress in drying latex films *Langmuir* **26** 3815–20
- [183] Xu Y, Engl W C, Jerison E R, Wallenstein K J, Hyland C, Wilen L A and Dufresne E R 2010 Imaging in-plane and normal stresses near an interface crack using traction force microscopy *Proc. Natl Acad. Sci.* **107** 14964–7
- [184] Jerison E R, Xu Y, Wilen L A and Dufresne E R 2011 Deformation of an elastic substrate by a three-phase contact line *Phys. Rev. Lett.* **106** 186103
- [185] German G K, Engl W C, Pashkovski E, Banerjee S, Xu Y, Mertz A F, Hyland C and Dufresne E R 2012 Heterogeneous drying stresses in stratum corneum *Biophys. J.* **102** 2424–32
- [186] Rosnagel S M, Gilstrap P and Rujkorakarn R 1982 Stress measurement in thin films by geometrical optics *J. Vac. Sci. Technol.* **21** 1045–6
- [187] Li J, Cabane B, Sztucki M, Gummel J and Goehring L 2012 Drying dip-coated colloidal films *Langmuir* **28** 200–8
- [188] Dingenouts N and Ballauff M 1998 Assessment of spatial order in dried latexes by small angle x-ray scattering *Macromolecules* **31** 7423–9
- [189] Rieger J, Hadicke E, Ley G and Lindner P 1992 Crystals made of close-packed polymeric spheres: a neutron scattering study on latex films *Phys. Rev. Lett.* **68** 2782–5
- [190] Joanicot M, Wong K, Richard J, Maquet J and Cabane B 1993 Ripening of cellular latex films *Macromolecules* **26** 3168–75
- [191] Mallegol J, Gorce J P, Dupont O, Jeynes C, McDonald P J and Keddie J 2002 Origins and effects of a surfactant excess near the surface of waterborne acrylic pressure sensitive adhesives *Langmuir* **18** 4478–87
- [192] Kunkel J P and Urban M W 1993 Surface and interfacial FT-IR spectroscopic studies of latexes: VIII. The effect of particle and copolymer composition on surfactant exudation in styrene-n-butyl acrylate copolymer latex films. *J. Appl. Polym. Sci.* **50** 1217–23
- [193] Zhao C L, Dobler F, Pith T, Holl Y and Lambla M 1989 Surface composition of coalesced acrylic latex films studied by XPs and SIMs *J. Colloid Interface Sci.* **128** 437–49
- [194] Kajiya T and Doi M 2008 Dynamics of drying process of polymer solution droplets: analysis of polymer transport and control of film profiles. *Nihon Reoroji Gakkaishi* **39** 17–28
- [195] Kajiya T, Kobayashi W, Okuzono T and Doi M 2010 Controlling profiles of polymer dots by switching between evaporation and condensation *Langmuir* **26** 10429–32